ΕΘΝΙΚΟ & ΚΑΠΟΔΙΣΤΡΙΑΚΟ

ΠΑΝΕΠΙΣΤΗΜΙΟ ΑΘΗΝΩΝ

ΤΜΗΜΑ ΦΥΣΙΚΗΣ

Τομέας Αστροφυσικής, Αστρονομίας & Μηχανικής

Μεταβατική αύξηση ενέργειας σε αστάθειες Holmboe

Ναβίτ Κ. Κωνσταντίνου

200820

Απρίλιος 2010

Acknowledgements

I would like to thank Petros Ioannou and Katerina. The first for being my teacher and my supervisor, for his help in all academic difficulties that came in my way and for his fruitful discussions, which are my main source of inspiration. The second for the times she cooked lunch, for her mental support through the last three years and for caring. Both of them for showing patience with me when needed.

Also, I would like to thank Alexander S. Onassis Public Benefit Foundation for funding the second year of my Master Degree education.

Contents

Chapter 1

Theoretical development

1.1 Introduction

In all problems of hydrodynamic stability the main question is whether a flow, that is a solution of the Navier-Stokes equations subject to specific boundary conditions, is stable or not if perturbed infinitesimally at some instant. It is exactly like the question of whether an equilibrium point in a dynamical system is stable or unstable when the equilibrium is perturbed at a point in time.

The state of the fluid is described in general by the velocity, density, temperature and pressure field over the volume occupied by the fluid. The usual procedure for asking whether an equilibrium state is stable or not starts by perturbing the mean fields (often called profiles in this text), then writing the Navier-Stokes equations of motion plus appropriate boundary conditions and linearizing in terms of the perturbation fields. We will be dealing with one-dimensional mean velocity flows that are unidirectional, this streamwise direction of flow will be taken as the x-axis. Moreover the flows we will consider vary only in the cross-stream direction, taken here

as the z-direction. The mean flows that will be considered are thus of the form $\vec{U} = U(z)\hat{x}$, where $\hat{x}$ is the unit vector in the x-direction. We will consider no dependence of the mean state on the third direction (the spanwise direction) y. Thus, also mean pressure, density and temperature will vary only in z-direction.

The system of linearized equations we will get will be homogeneous in x, y and t and therefore the perturbations can be written as a sum of Fourier modes with dependance $e^{i(kx+\ell y)-ikct}$. After this expansion we are left with an eigenvalue problem with eigenvalue c for every choice of the pair (k, ℓ). As we will see in hydrodynamics c is in general complex, and if $c \equiv c_r + ic_i$ then the (k, ℓ) mode is of form

$$e^{kc_i t} e^{i(kx+\ell y-kc_r t)}$$

i.e. it is a wave which propagates in the direction (k, ℓ) with phase velocity $kc_r/\sqrt{k^2+\ell^2}$ while growing (or decaying) at the exponential rate kc_i.

We say that the flow is *modally stable* if and only if $c_i \equiv \Im(c)$ is less or equal to zero for all choices of (k, ℓ). Otherwise the flow is *modally unstable*. This procedure is presented in more detail in Section 1.2.

There is a theorem by Squire [9], extended by Yih [13] to include stratification, that states that for any three dimensional perturbations in two-dimensional flows corresponds a two-dimensional perturbation that has larger growth rate. Stated otherwise, growth rates kc_i resulting from two-dimensional perturbations will be always greater or equal to the ones resulting from three-dimensional ones. Thus, if we investigate the modal stability of a flow it is enough only to limit our search to dimensional perturbations that have $\ell = 0$, two-dimensional perturbations. Note that

Squire's theorem does not constrain superpositions of modes and as a result it is a time infinity asymptotic result.

1.1.1 Couette flow

The Couette is a flow with a constant shear, $\mathrm{d}U_0/\mathrm{d}z$, as can be seen on Figure 1.1(a). It has been shown that this flow is always stable, in a bounded or an unbounded domain. A necessary condition for the instability of bounded, parallel shear flows is the Rayleigh criterion which demands that the velocity flow should have at least one inflection point, that is a point in the domain where $\mathrm{d}^2U_0/\mathrm{d}z^2$ changes sign (see Drazin and Reid [2]).

1.1.2 Kelvin-Helmholtz instability

Let us first study, or better describe, the Kelvin-Helmholtz instability. This occurs when there is a sudden jump in the velocity profile. We will discuss the inviscid variant of this instability (the instability has also a viscous counterpart that is qualitatively similar). In the inviscid limit this jump may be idealized as a step function, which in the absence of viscosity is an equilibrium of the Euler equations (actually in the inviscid hydrodynamic limit any mean flow $U(z)$ is an equilibrium). If we choose our reference system appropriately then the velocity jump can be centered so that above the velocity discontinuity the velocity is U and below -U (see Figure 1.1(b)). The main vorticity of this flow in the y-direction (spanwise) is everywhere zero except from the surface $z = 0$ where it is a positive delta function. That's why many times this configuration is also called vortex sheet configuration.

There is a very special property of vorticity dynamics in inviscid fluids,

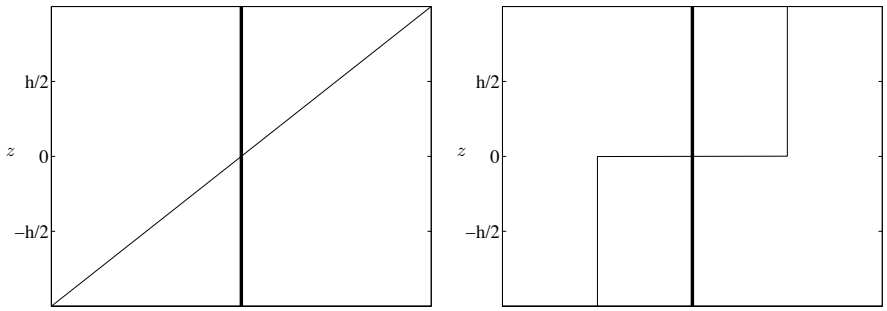

1.1(a): Couette

1.1(b): Kelvin-Helmholtz

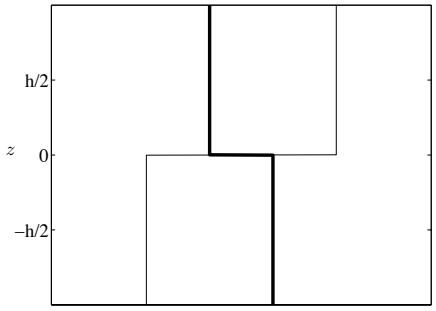

1.1(c): Kelvin-Helmholtz stratified

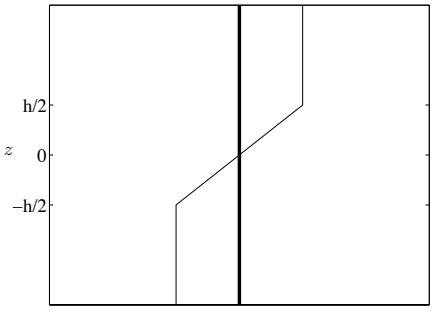

1.1(d): Rayleigh

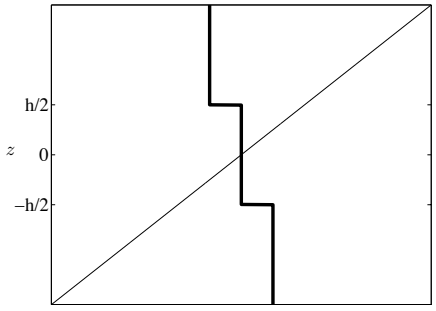

1.1(e): Taylor

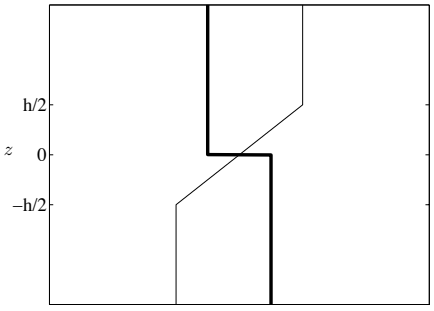

1.1(f): Holmboe

Figure 1.1: Main velocity (thin lines) and density (thick lines) for various piecewise profiles.

that states that vorticity lines behave exactly as material lines. For more detailed description see for example in Batchelor [1]. In other words, if we paint a vorticity line with a dye of different color of the fluid, this line will always stay a solid line.

For each streamwise wavenumber k we find that there is a pair of modes with the dispersion relation $c(k) = \pm iU$, independent of k. Therefore this flow is always unstable. The mechanism responsible for the instability can be understood in terms of vorticity dynamics. In solving the stability problem above we end up with only two perturbation fields from which the rest can be derived, the y-vorticity and the displacement of the initial separating surface. Furthermore if the latter is of a sinusoidal form then the former is of the same form, but $\pi/2$ ahead in phase if $c = +iU$ (if $c = -iU$ then displacement is $\pi/2$ ahead of phase of the vorticity). In Figure 1.2 we plot the displacement as a sinusoidal surface and also the vorticity of the perturbations as the thickness of the surface line (thick lines means positive vorticity). Points like C have maximum positive vorticity, and so induce velocities like the clockwise arrows around C which tend to bring point B, the highest point of the separation surface even higher.

The growth rate kc_i for this discontinuous profile is kU and so it grows linearly with k, implying an ultraviolet catastrophe, as the growth rate becomes nominally infinite as $k \to +\infty$ for perturbations with very small wavelength. This ultraviolet catastrophe is a manifestation of the inviscid dynamics. Inclusion of viscosity would damp this high wavenumbers and would cure this ultraviolet catastrophe, also viscosity would also smooth out the discontinuity which as we will see even in the presence of inviscid renders stable the ultraviolet spectrum. A step towards treating an inviscid

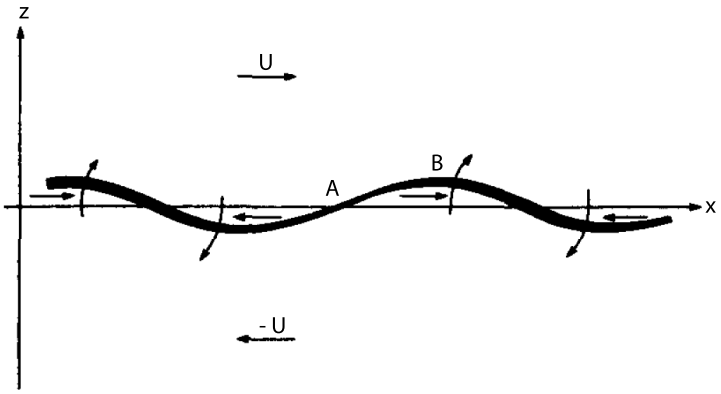

Figure 1.2: The instability mechanism for the Kelvin-Helmholtz instability. (after Batchelor [1], fig. 7.1.3)

but smoothed out velocity profile is achieved with the piecewise linear profile studied by Rayleigh.

1.1.3 Rayleigh instability

Rayleigh studied first the profile of Figure 1.1(d), in which the velocity jump is smoothed over a region h. The mean vorticity is piecewise constant with equal and opposite discontinuities at $z = \pm h/2$.

In general, for piecewise profiles each discontinuity in the vorticity gives rise to a so called *vorticity* mode and each discontinuity in main density supports two *density* modes. The vorticity modes are centered at the points where the shear is discontinuous, while the density modes where the density has a discontinuity. They are both of the form $e^{-k|z-z_c|}$, (z_c is the discontinuity level) and hence have skin depths of $1/k$ and are trapped next to the discontinuity.

Thus, Rayleigh's profile has two vorticity modes, one for each shear discontinuity. The spectrum is seen in Figure 1.3. By solving explicitly the problem we find that for large wavenumbers (short wavelengths) the

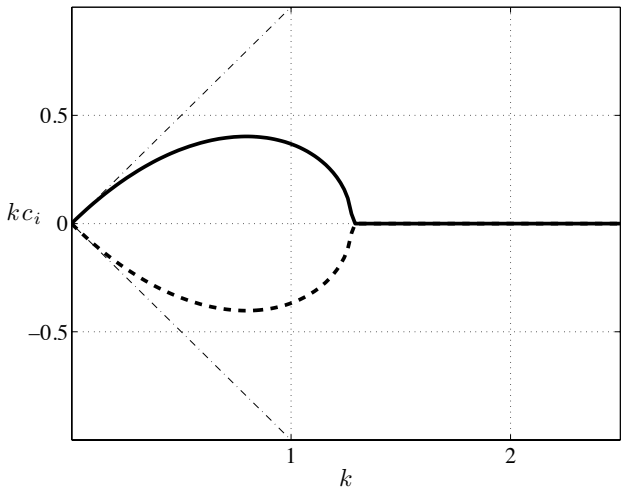

1.3(a): growth rates

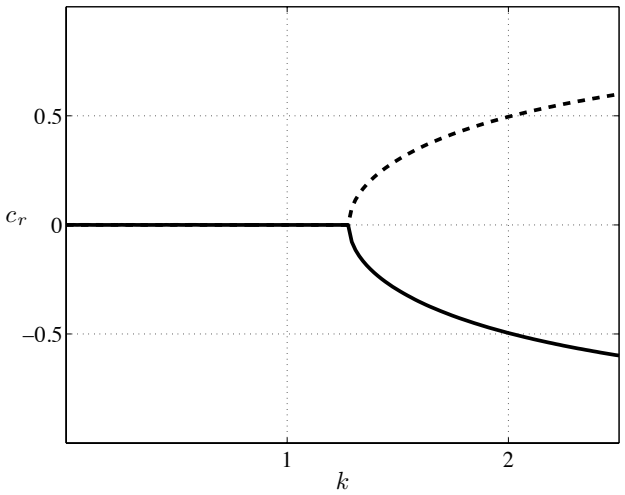

1.3(b): phase velocities

Figure 1.3: The spectrum for the Rayleigh profile of Figure 1.1(d). Growth rates of the two modes (solid and dashed lines) are seen in (a) and phase velocities in (b). In (a) we plot the grow rates associated to the Kelvin-Helmholtz profile (Figure 1.1(b)), $\pm kU$ (dash-dot lines). We see that $k_c \approx 1.3$. For $k < k_c$ we have a conjugate pair of positive and a negative growth rates corresponding to the unstable and stable mode that propagate with zero phase velocity. For $k > k_c$ the two discrete modes are neutral ($kc_i = 0$) and propagate with equal and opposite phase velocity which tends to $\pm U$ as $k \to +\infty$. We see that for for small wavenumbers growth rates approach the ones of the Kelvin-Helmhotlz profile. Wavenumbers have been non-dimensionalized with $1/h$ and velocities with U.

flow is stable, that is c is real. It is like the two modes "do not see" each other, or in an other view, if the wavenumber is very large, that is the wavelength is very small, the waves can only "see" the middle part of the profile, which is like Couette flow and as a result the flow is stable. There is a critical value k_c such that for wavenumbers less than k_c mode interactions becomes strong, or the wavelength become so large that can feel the discontinuities of the main vorticity, and so a pair of stationary (zero phase velocity) "Kelvin-Helmholtz" modes are produced, a growing one and a decaying one (instability). For very small wavenumbers the waves do not see the linear transition between the two velocities, and behave as if there was a velocity jump and they exhibit the instability associated with the Kelvin-Helmholtz profile for which the growth rate is proportional to kU.

1.1.4 Kelvin-Helmhotz instability with stratification

We can study the Kelvin-Helmholtz instability if we further include a density jump in a way that the fluid is stably stratified, that is lighter fluid on top of denser fluid (see Figure 1.1(c)). We would expect that this factor now reduces the instability, since perturbations would need to spend potential energy in lifting a bulb of the lower fluid into the upper area. Indeed, if we explicitly solve the problem, the dispersion relation now becomes:

$$c = -\frac{1-\varepsilon}{1+\varepsilon}U \pm i\sqrt{\frac{4\varepsilon U^2}{(1+\varepsilon)^2} - \frac{g}{k}\frac{1-\varepsilon}{1+\varepsilon}} \tag{1.1}$$

where g is the gravity acceleration and ε is the ratio of the density of the top over the lower fluid, $\varepsilon = \rho_1/\rho_2$. The limit $\varepsilon = 1$ corresponds to the

unstratified case $c = \pm iU$. If there is only the density discontinuity, that is $U = 0$, then we have the two stable, internal wave modes,

$$c = \pm\sqrt{\frac{g}{k}\frac{1-\varepsilon}{1+\varepsilon}} \tag{1.2}$$

or for the extremely stratified case of $\varepsilon = 0$, that is infinitely large difference of densities of the two fluids, we have the surface wave modes, $c = \pm\sqrt{g/k}$. (Sea waves correspond to $\varepsilon \approx 10^{-3}$.)

Now, for finite values of U and $\sqrt{g/k}$ there is always for each streamwise wavenumber k a critical value ε_c,

$$\varepsilon_c = -2\frac{U^2}{g/k} + \sqrt{\left(2\frac{U^2}{g/k}\right)^2 + 1} \tag{1.3}$$

that for $\varepsilon < \varepsilon_c$ the flow gets stabilized. From this observation we see that what we expected is true. The stratification indeed stabilizes the flow. Going back to the dispersion relation, we can also see that for a fixed value of ε we have a critical value of $k = k_c$,

$$k_c = \frac{1-\varepsilon^2}{\varepsilon}\frac{g}{4U^2} \tag{1.4}$$

for which we have stability for $k < k_c$ and instability for $k > k_c$.

We plot in Figure 1.4 the growth rates and the phase velocities of the two modes for the unstratified case, $\varepsilon = 1$ together with stratification of $\varepsilon = 0.5$ and $\varepsilon = 0.1$.

1.1.5 Taylor instability

Taylor studied [10] a profile with two density jumps imposed on constant shear velocity profile, seen on Figure 1.1(e). Now four modes gravity

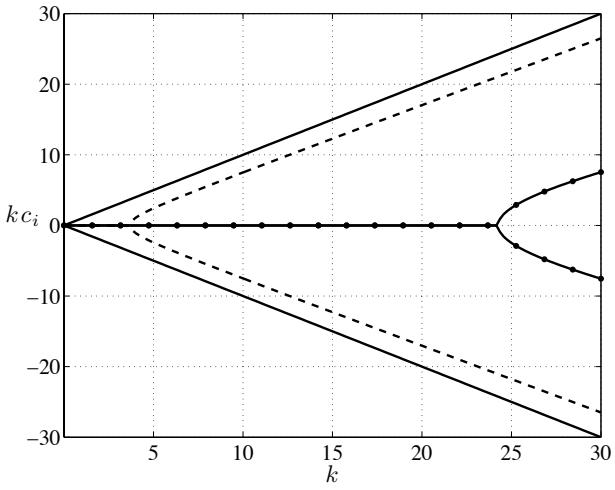

1.4(a): growth rates

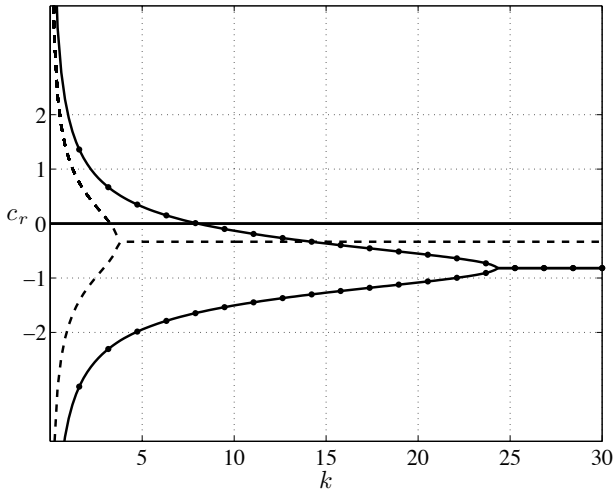

1.4(b): phase velocities

Figure 1.4: The spectrum for the Kelvin-Helmholtz stratified profile of Figure 1.1(c). Growth rates of the two modes (solid and dashed lines) are seen in (a) and phase velocities in (b) for $\varepsilon = 1$ (solid), $\varepsilon = 0.5$ (dashed) and $\varepsilon = 0.1$ (solid dotted). We see that there always exists a wavenumber k_c such that for $k > k_c$ we have a conjugate pair of positive and a negative growth rates corresponding to the unstable and stable mode that propagate with zero phase velocity and for $k < k_c$ the two discrete modes are neutral ($kc_i = 0$) and propagate with equal and opposite phase velocity. Wavenumbers have been non-dimensionalized with $1/h$ and velocities with U.

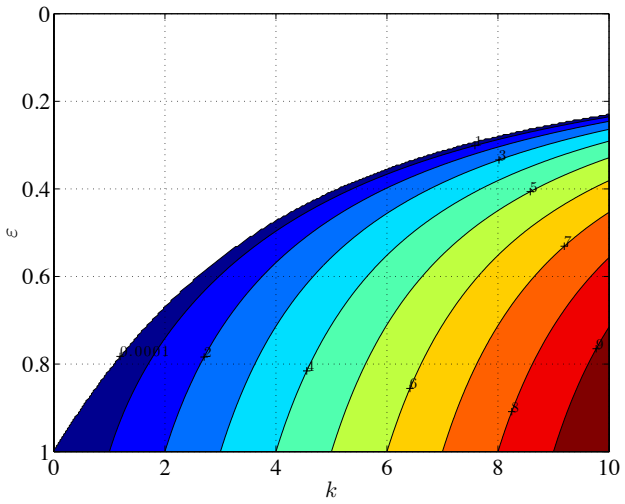

1.5(a): Kelvin-Helmholtz stratified

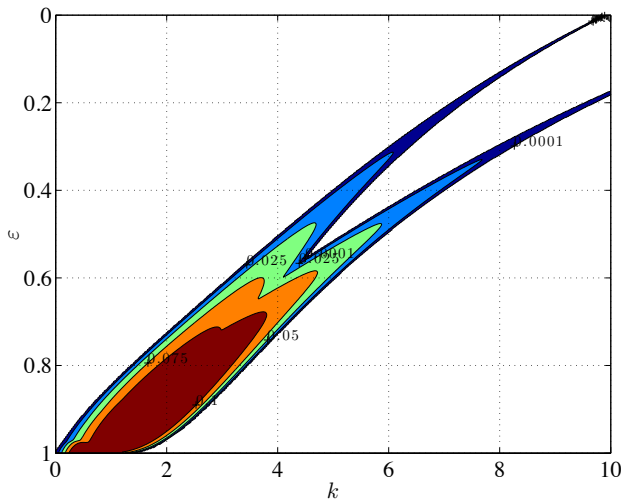

1.5(b): Holmboe

Figure 1.5: Maximum growth rate kc_i versus streamwise wavenumber k and density ratio ε for (a) Kelvin-Helmholtz stratified profile (Figure 1.1(c)) and (b) Holmboe's profile (Figure 1.1(f)). We see that for the Holmboe case there are wavenumbers (i.e. $k = 4$) that are stable for the unstratified case ($\varepsilon = 1$) but become unstable when stratification in included.

modes exist propagating with equal and opposite velocity relative to the velocity at the density steps. For long wavenumbers they do not interact and there is stability. For shorter wavenumbers though, less than a critical values, two of the modes merge and form a stationary pair of a stable and unstable mode.

1.1.6 Holmboe instability

Holmboe instabilities occur whenever there is both velocity and density jumps, but the former accomplished in a greater region than the latter. The ratio of these two regions will be denoted by R. Holmboe's prototype profile is seen in Figure 1.1(f), where for this case $R = \infty$. We can see the two shear discontinuities and a density discontinuity in between them. In this case a counterintuitive thing happens. Stratification induces instability for a range of streamwise wavenumbers for which the flow would have been stable in the unstratified case. Thus, by this mechanism, we can have instability, and hence mixing of the two fluids, for very high values of stratification. It is the interaction of each of the vorticity modes with one of each of the gravity modes that produces two pairs of a decaying and a growing mode, one pair with phase velocity going to the left and the other pair going to the right.

1.1.7 Finite amplitude

Stability characteristics of the above instabilities have been obtained after linearization. But, when a flow is unstable, it means that the fields amplitude will grow with time, reaching a point that the linearization approximation will not be valid. Our linearized equations will not be able to give us an adequate description of the evolution of the flow after-

1.6(a): Rayleigh or Kelvin-Helmholtz

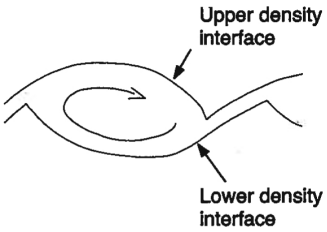

1.6(b): Taylor

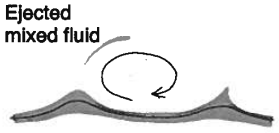

1.6(c): Holmboe

Figure 1.6: The finite amplitude evolutions of the three basic stratified instabilities: Rayleigh or Kelvin-Helmholtz (a), Taylor (b) and Holmboe (c). (after Tedford [11], fig. 3)

wards. One must proceed with integration of the full nonlinear equations of motion by direct numerical simulations (DNS). The latter as well as experiments have revealed the behavior, summarized in Figure 1.6, for the finite amplitude instabilities described previously.

Rayleigh instability at finite amplitudes forms spiralling billows like Figure 1.6(a). As the instability grows, neighboring billows interact and combine ('pair') to form a new billow with twice the wavelength and increased amplitude. This procedure continues until wavelength reaches the boundaries of the fluid. The Taylor instability has at finite amplitude a series of vortices located between the two density interfaces (the upper and lower density interfaces) (see Figure 1.6(b)). Unlike Rayleigh instabilities, their development does not cause complete overturning of the density interface. The Holmboe instability features cusping waves somewhat resembling surface water waves (see Figure 1.6(c)). At the cusp of

the wave mixed fluid of intermediate density accumulates, and eventually being ejected into the upper density layer. Again there is not a complete overturning of the density interface.

1.2 Formulation of the problem

We begin by studying the stability of an inviscid, one dimensional flow under two dimensional perturbations. With asterisks $*$ dimensional quantities are denoted. Perturbations about a mean zonal flow $U_0^*(z^*)$ in an incompressible, stratified, Boussinesq fluid obey the equations:

$$\rho_m^* \left(\frac{\partial}{\partial t^*} + U_0^* \frac{\partial}{\partial x^*} \right) u^* = -w^* \frac{\mathrm{d}U_0^*}{\mathrm{d}z^*} - \frac{\partial p^*}{\partial x^*} \tag{1.5.a}$$

$$\rho_m^* \left(\frac{\partial}{\partial t^*} + U_0^* \frac{\partial}{\partial x^*} \right) w^* = -\frac{\partial p^*}{\partial z^*} - g\varrho^* \tag{1.5.b}$$

$$\left(\frac{\partial}{\partial t^*} + U_0^* \frac{\partial}{\partial x^*} \right) \varrho^* = -\frac{\mathrm{d}\varrho_0^*}{\mathrm{d}z^*} w^* \tag{1.5.c}$$

$$\frac{\partial u^*}{\partial x^*} + \frac{\partial w^*}{\partial z^*} = 0 \tag{1.5.d}$$

In the above u^*, w^* are the perturbation velocities in the streamwise (x) and vertical (z) direction, ϱ^* is the perturbation of the density, p^* is the pressure and g is the gravitational acceleration. The density of the fluid has been decomposed as: $\rho^* \equiv \rho_m^* + \rho_0^*(z) + \varrho^*(x,z,t)$ and furthermore, according to the Boussinesq approximation, $|\rho_0^*| \ll \rho_m^*$ and $|\varrho^*| \ll \rho_m^*$. We will assume vanishing boundary conditions at the boundaries z_1^* and z_2^* and also periodic boundary conditions in the streamwise direction. A thorough discussion and derivation of the Navier-Stokes equations, their linearization and the approximations are beyond the scope of this essay. Refer to classical books in fluid dynamics [1] and hydrodynamic stability [2].

We will convert our equations to a non-dimensional form using as length scale h_0, the typical length of the variation of the velocity, velocity scale $\tilde{u} = U_0^*(+\infty) - U_0^*(-\infty)$ which by right choise of our coordinate system will be assumed positive, and density scale $\tilde{\rho} = \rho^*(-\infty) - \rho^*(+\infty)$. We will only deal with stably stratified fluid, that is $\tilde{\rho} > 0$. For time unit we will use the advective time scale, $h_0/\tilde{u}$ and pressure will be measured in units of $\rho_m^* \tilde{u}^2$ and wavenumbers we will be scaled with $1/h_0$.

The Brunt-Väisälä frequency, N^* is defined (in the Boussinesq context) as $N^{*2}(z^*) = -(g/\rho_m^*)\, \mathrm{d}\rho_0^*/\mathrm{d}z^*$. If N^{*2} is positive then we say that the fluid is stably stratified (for example oil on top of water is stably stratified) and then N^* is the local frequency of the oscillations that a bulb of fluid will do if we displace it a bit from its initial height. If N^{*2} is negative then we say that the fluid is unstably stratified (for example water on top of oil). We will only consider stably stratified fluids in this discussion.

The Richarson number is defined as the Brunt-Väisälä frequency squared over the local shear squared, $\mathrm{Ri}(z^*) = N^{*2}(z^*) \,/\, (\mathrm{d}U_0^*/\mathrm{d}z^*)^2$. The Richarson number is the ratio of the square of two time scales: the time scale of the shear dynamics over the time scale associated with gravity wave oscillation. Large Ri means that the gravity oscillations are far faster than the dynamics of shear, implying that stratification dominates and the perturbations behave as internal gravity waves in the absence of shear. Small Ri implies dominance of shear dynamics over the dynamics implied by the stratification. Moreover, the non-dimensional quantity J, connected with Richarson number, is denoted to be:

$$J = \frac{g\tilde{\rho}h_0}{\rho_m^* \tilde{u}^2} \tag{1.6}$$

A necessary condition proven by Miles [7] and Howard [5], also known as the Miles & Howard criterion, for the flow to be unstable is that the Richarson number must be less than $1/4$ somewhere in the domain of the flow. In Appendix C we give the proof of this theorem.

The non-dimensional version of (1.5.c) is:

$$\left(\frac{\partial}{\partial t} + U_0 \frac{\partial}{\partial x}\right) \varrho = -\frac{\mathrm{d}\rho_0}{\mathrm{d}z}\, w \tag{1.7}$$

We can define the vertical displacement η of every point due to the perturbation velocity field by requiring that the substantial derivative of it at every point being equal to the vertical velocity, w,

$$\left(\frac{\partial}{\partial t} + U_0 \frac{\partial}{\partial x}\right) \eta = w \tag{1.8}$$

Now, from (1.7) we can see that η and ϱ are related by

$$\varrho = -\left(\mathrm{d}\rho_0/\mathrm{d}z\right) \eta \tag{1.9}$$

and thus η can serve as a state variable in the place of ϱ. With these conventions, equations (1.5), become:

$$\left(\frac{\partial}{\partial t} + U_0 \frac{\partial}{\partial x}\right) u = -\frac{\mathrm{d}U_0}{\mathrm{d}z} w - \frac{\partial p}{\partial x} \tag{1.10.a}$$

$$\left(\frac{\partial}{\partial t} + U_0 \frac{\partial}{\partial x}\right) w = J \frac{\mathrm{d}\rho_0}{\mathrm{d}z} \eta - \frac{\partial p}{\partial z} \tag{1.10.b}$$

$$\left(\frac{\partial}{\partial t} + U_0 \frac{\partial}{\partial x}\right) \eta = w \tag{1.10.c}$$

$$\frac{\partial u}{\partial x} + \frac{\partial w}{\partial z} = 0 \tag{1.10.d}$$

or in a more concise form as

$$L\phi = 0 \tag{1.11}$$

where the state is $\phi = [u, w, \eta, p]^T$ and L is:

$$L = \begin{bmatrix} \partial_t + U_0\partial_x & \mathrm{d}U_0/\mathrm{d}z & 0 & \partial_x \\ 0 & \partial_t + U_0\partial_x & -J\,(\mathrm{d}\rho_0/\mathrm{d}z) & \partial_z \\ 0 & -1 & \partial_t + U_0\partial_x & 0 \\ \partial_x & \partial_z & 0 & 0 \end{bmatrix} \tag{1.12}$$

Our dynamical system (1.10) concists of three dynamical equations (1.10.a, 1.10.b and 1.10.c) and a constraint, (1.10.d). Thus, by using a streamfunction ψ to describe the velocity field:

$$u = \frac{\partial \psi}{\partial z} \tag{1.13.a}$$

$$w = -\frac{\partial \psi}{\partial x} \tag{1.13.b}$$

the system can be reduced to two equations.

$$\frac{\partial\, \mathbf{x}}{\partial t} = \mathbb{A}\, \mathbf{x} \tag{1.14}$$

with $\mathbf{x} = [\psi, \eta]^{\mathrm{T}}$ as our state vector. The dynamical system (1.14) is homogeneous in x and therefore the perturbations can be written as a sum of Fourier modes of the form $x_k(z,t)e^{ikx}$. Each mode is governed by:

$$\frac{d}{dt}\mathbf{x}_k = \mathbb{A}^{(k)}\, \mathbf{x}_k \tag{1.15}$$

where $\mathbb{A}^{(k)}$ is:

$$\mathbb{A}^{(k)} = \begin{bmatrix} \Delta^{-1}\left(-ikU_0\Delta + ik\dfrac{\mathrm{d}^2U_0}{\mathrm{d}z^2}\right) & -ikJ\Delta^{-1}\dfrac{\mathrm{d}\rho_0}{\mathrm{d}z} \\ -ik & -ikU_0 \end{bmatrix} \tag{1.16}$$

In the above Δ denotes the two dimensional Laplacian, $\Delta = \partial^2_{xx} + \partial^2_{yy}$, and Δ^{-1} is the inverse Laplacian, the inversion being made possible and unique by imposing the appropriate boundary conditions on the upper and lower boundary.

One can proceed further and reduce the system into a second order partial differential equation for ψ:

$$\left(\frac{\partial}{\partial t} + U_0\frac{\partial}{\partial x}\right)^2 \Delta\psi - \frac{\mathrm{d}^2U_0}{\mathrm{d}z^2}\left(\frac{\partial}{\partial t} + U_0\frac{\partial}{\partial x}\right)\frac{\partial\psi}{\partial x} - J\frac{\mathrm{d}\rho_0}{\mathrm{d}z}\frac{\partial^2\psi}{\partial x^2} = 0 \tag{1.17}$$

The above equation is the generalization of the Rayleigh equation that includes stratification and is called the Taylor-Goldstein equation.

1.3 Energetics

To obtain an energy equation we proceed as Miles [7] by multiplying equations (1.10.a) and (1.10.b) by u and w respectively, substituting w from (1.10.c) in the $J\,(\mathrm{d}\rho_0/\mathrm{d}z)\,w\eta$ term and multiply (1.10.d) by p. We add the results and intergrate over x and z domains. This results to:

$$\begin{aligned} \frac{\mathrm{d}}{\mathrm{d}t}\int_{z_1}^{z_2} dz\ \overline{\frac{1}{2}\left(u^2+w^2\right) + \frac{1}{2}\left(-\frac{\mathrm{d}\rho_0}{\mathrm{d}z}\right)J\,\eta^2} = \\ -\int_{z_1}^{z_2} dz\ \overline{uw\frac{\mathrm{d}U_0}{\mathrm{d}z}} - \int_{z_1}^{z_2} dz\ \overline{\frac{\partial}{\partial x}(pu) + \frac{\partial}{\partial z}(pw)} \end{aligned} \tag{1.18}$$

where overline denotes integration in the x domain. The last set of integrals die with the assumed boundary conditions. This fact is equivalent that no pressure force work is being done to the perturbation flow by external pressures on the boundaries of the fluid. If we next denote by bar integrals on x-domain, the above equation can be written:

$$\frac{\mathrm{d}}{\mathrm{d}t}\left(T+V\right)=Q \tag{1.19}$$

where T is the total kinetic energy of the perturbations over the flow domain,

$$T=\frac{1}{2}\int_{z_1}^{z_2}dz\;\overline{u^2+w^2} \tag{1.20}$$

V is the potential energy,

$$V=\frac{1}{2}J\int_{z_1}^{z_2}dz\;\left(-\frac{\mathrm{d}\rho_0}{\mathrm{d}z}\right)\overline{\eta^2} \tag{1.21}$$

and Q,

$$Q=-\int_{z_1}^{z_2}dz\;\overline{uw}\,\frac{\mathrm{d}U_0}{\mathrm{d}z} \tag{1.22}$$

determines the time rate of energy flow from the mean-flow to the perturbation field.

The total energy of the perturbations, integrated over whole space, is given by $E=T+V$.

A geometrical interpretation of the conditions under which perturbations gain energy from the mean flow can be readily given if we note that

(1.22) can be written in terms of the perturbation streamfunctions as:

$$Q = \int_{z_1}^{z_2} dz \, \overline{\frac{\partial \psi}{\partial x} \frac{\partial \psi}{\partial z}} \frac{\mathrm{d}U_0}{\mathrm{d}z} \tag{1.23}$$

The streamfunction ψ depends on x and z. Its differential is given by

$$\mathrm{d}\psi = \frac{\partial \psi}{\partial x}\mathrm{d}x + \frac{\partial \psi}{\partial z}\mathrm{d}z$$

and on a surface of constant ψ this is equal to zero. This means that the slopes of contours of constant ψ satisfy the relation:

$$\frac{\partial \psi}{\partial x} / \frac{\partial \psi}{\partial z} = - \left. \frac{\partial z}{\partial x} \right|_{\psi = \mathrm{c}} \tag{1.24}$$

which when inserted in (1.23) gives:

$$Q = - \int_{z_1}^{z_2} dz \, \overline{\left(\frac{\partial \psi}{\partial z} \right)^2 \left. \frac{\partial z}{\partial x} \right|_{\psi = \mathrm{c}}} \frac{\mathrm{d}U_0}{\mathrm{d}z} \tag{1.25}$$

This means that for areas with positive shear, $(\mathrm{d}U_0/\mathrm{d}z > 0)$, Q behaves as dissipation when the ψ surfaces slope forward i.e. $\partial z/\partial x > 0$ (see Figure 1.7(a)) and Q behaves as a source of energy when ψ surfaces slope backward, i.e. $\partial z/\partial x < 0$ (see Figure 1.7(b)).

In order to evaluate the kinetic and potential energy we expand the fields as Fourier integrals:

$$\varphi(x, z, t) = \int_{-\infty}^{+\infty} dk \, \hat{\varphi}_k(z) e^{ikx} \tag{1.26}$$

Because only the real part is physically realizable care must be taken in evaluating the kinetic and potential energy which depend quadratically

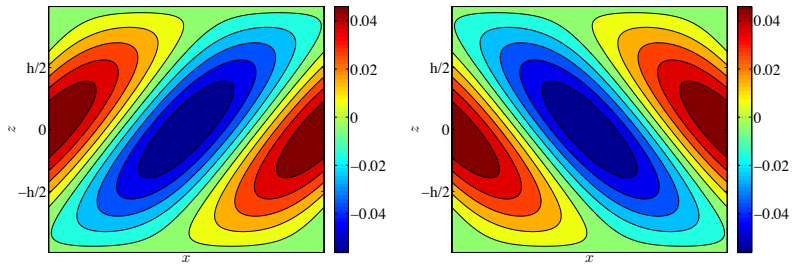

1.7(a): ψ resulting in decrease of total energy

1.7(b): ψ resulting in increase of total energy

Figure 1.7: Examples of streamfunction contours that will lead to term Q, (1.25), giving increase or decrease of total energy.

on the perturbation fields. In quadratic quantities we must explicitely write the real part of the field, and by doing so it can be easily shown that the x average of the product of two fields[1] $\varphi_1 = \hat{\varphi}_1 e^{ikx}$ and $\varphi_2 = \hat{\varphi}_2 e^{ikx}$ is:

$$\overline{\Re(\varphi_1)\Re(\varphi_2)} = \frac{1}{2}\Re\left(\hat{\varphi}_1^* \hat{\varphi}_2\right) \tag{1.27}$$

and also doing an integration by parts and using the boundary conditions, we can reduce the expressions for kinetic and potential energy into:

$$T = \frac{1}{4}\int_{z_1}^{z_2} dz\ \hat{\psi}^* \Delta \hat{\psi} \tag{1.28.a}$$

$$V = \frac{1}{4} J \int_{z_1}^{z_2} dz\ \left(-\frac{\mathrm{d}\rho_0}{\mathrm{d}z}\right) \hat{\eta}^* \hat{\eta} \tag{1.28.b}$$

1.4 Non-normal growth

The nature of the evolution of the dynamics depends strongly on the nature of the dynamical operator $\mathbb{A}$ (see equation (1.14)). Whether or not $\mathbb{A}$ is a normal or non-normal operator will play significant role in the

[1] with the subscript k omitted

transient evolution and optimal excitation of the system. A systematic theory describing this part of the dynamics was developed by Farrell and Ioannou [3]. Nonnormality measures the degree of non-commutativity of $\mathbb{A}$ with its adjoint, $\mathbb{A}^\dagger$. To have a proper definition of an adjoint operator one must first have an inner product usually defined by a positive definite hermitian form $\mathbb{M}$, that is, $(\mathbf{x},\mathbf{x})_\mathrm{M} \equiv \mathbf{x}^\dagger\mathbb{M}\mathbf{x}$ and the norm of $\mathbf{x}$ defined as $\|\mathbf{x}\|_\mathrm{M} = \left(\mathbf{x}^\dagger\mathbb{M}\mathbf{x}\right)^{1/2}$. In most physical cases $\mathbb{M}$ is the energy metric so that $\|\mathbf{x}\|^2_\mathrm{M}$ measures the energy of state $\mathbf{x}$. Without loss of generality we can consider that the norm is euclidean because if we set $\mathbf{y} = \mathbb{M}^{1/2}\mathbf{x}$ then the evolution of $\mathbf{y}$ is controlled by:

$$\frac{\partial\,\mathbf{y}}{\partial t} = \mathbb{M}^{1/2}\mathbb{A}\mathbb{M}^{-1/2}\mathbf{y} \equiv \mathbb{A}_\mathrm{M}\,\mathbf{y} \tag{1.29}$$

while the norm of the state $\mathbf{y}$ will be given by $\|\mathbf{y}\|^2 \equiv \mathbf{y}^\dagger\mathbf{y} = \mathbf{x}^\dagger\mathbb{M}\mathbf{x} = \|\mathbf{x}\|^2_\mathrm{M}$. Let us assume for now that such transformation of coordinates has been made and so, in the system (1.14) all norms are Euclidean[2].

The adjoint operator $\mathbb{A}^\dagger$ is defined such that for any two state vectors $\mathbf{u}$ and $\mathbf{v}$ we have

$$(\mathbf{v},\mathbb{A}\mathbf{u}) = \left(\mathbb{A}^\dagger\mathbf{v},\mathbf{u}\right) \tag{1.30}$$

Among the properties of the adjoint operator $\mathbb{A}^\dagger$ is that its spectrum is the complex conjugate of that of $\mathbb{A}$, that is:

$$\lambda \in \Lambda\left(\mathbb{A}\right) \Leftrightarrow \lambda^* \in \Lambda\left(\mathbb{A}^\dagger\right)$$

where we have denoted with Λ the spectum of an operator, that is the set of all its eigenvalues. Furthermore, eigenvectors of $\mathbb{A}$ corresponding

[2] and therefore we will omit the subscript M from the operators

to eigenvalue λ are orthogonal to all eigenvectors of $\mathbb{A}^\dagger$ that correspond to eigenvalues different from λ^*. This is the so called biorthogonality relation.

$$\left.\begin{aligned}\mathbb{A}\,\mathbf{u}^{(i)} &= \lambda_i\,\mathbf{u}^{(i)}\\ \mathbb{A}^\dagger\,\mathbf{v}^{(i)} &= \lambda_i^*\,\mathbf{v}^{(i)}\end{aligned}\right\} \Longrightarrow \left(\mathbf{v}^{(i)},\mathbf{u}^{(j)}\right) = 0 \quad \text{for } i \neq j \tag{1.31}$$

If $\mathbb{A}$ is normal then vectors $\mathbf{u}^{(i)}$ and $\mathbf{v}^{(i)}$ coincide, therefore it is said that $\mathbb{A}$ has a complete orthonormal basis. Otherwise the eigenvectors of $\mathbb{A}$ form just a complete basis, which is not orthonormal, but which is orthonormal to the eigenvectors of $\mathbb{A}^\dagger$. (You can refer to Appendix A for proofs of the above statements.)

Let us define the growth $\sigma(t)$ of an initial state $\mathbf{y}(0)$ over time t to be the ratio:

$$\begin{aligned}\sigma^2(t) &= \frac{(\mathbf{y}(t)\,,\,\mathbf{y}(t))}{(\mathbf{y}(0),\mathbf{y}(0))}\\ &= \frac{\left(e^{\mathbb{A}t}\mathbf{y}(0)\,,\,e^{\mathbb{A}t}\mathbf{y}(0)\right)}{(\mathbf{y}(0),\mathbf{y}(0))}\\ &= \frac{\left(\mathbf{y}(0)\,,\,e^{\mathbb{A}^\dagger t}e^{\mathbb{A}t}\mathbf{y}(0)\right)}{(\mathbf{y}(0),\mathbf{y}(0))}\end{aligned} \tag{1.32}$$

where in the last line we used the definition of the adjoint operator. Thus the maximum possible $\sigma^2(t)$ will be given by the maximum eigenvalue of the positive operator $e^{\mathbb{A}^\dagger t}e^{\mathbb{A}t}$ or equivalently by the square of the maximum singular value of $e^{\mathbb{A}t}$ (see Appendix B). The last is also many times referred as the norm squared of the operator $e^{\mathbb{A}t}$, where the norm of an operator Φ is defined as:

$$\|\Phi\|^2 = \max_{\mathbf{x}} \frac{(\Phi\mathbf{x}\,,\,\Phi\mathbf{x})}{(\mathbf{x},\mathbf{x})} \tag{1.33}$$

Now, when $\mathbb{A}$ is normal we have:

$$\exp\left(\mathbb{A}^{\dagger}t\right)\exp\left(\mathbb{A}t\right)=\exp\left[\left(\mathbb{A}^{\dagger}+\mathbb{A}\right)t\right] \tag{1.34}$$

and since $\mathbb{A}$ and $\mathbb{A}^{\dagger}$ have complex conjugate spectrums, we get that σ is bounded by:

$$e^{\lambda_{\min}^{\mathrm{R}}(\mathbb{A})t}\leq\sigma\leq e^{\lambda_{\max}^{\mathrm{R}}(\mathbb{A})t} \tag{1.35}$$

where $\lambda_{\min}^{\mathrm{R}}\left(\mathbb{A}\right)$ and $\lambda_{\max}^{\mathrm{R}}\left(\mathbb{A}\right)$ corresponds to the minimum and maximum real part of the eigenvalues of $\mathbb{A}$, respectively. The equality in the above bounds can be achieved if we use as initial state $\mathbf{u}(0)$ the eigenvector that corresponds to the eigenvalue with minimum or maximum real part respectively. The latter is due to the fact that $\mathbb{A}$ commutes with $\mathbb{A}^{\dagger}$ and thus $e^{\mathbb{A}^{\dagger}t}e^{\mathbb{A}t}$ has common eigenvectors with $\mathbb{A}$.

When $\mathbb{A}$ is non-normal, equation (1.34) does not hold. What does hold is the known Baker-Haussdorf-Campell formula:

$$\exp\left(\mathbb{A}^{\dagger}t\right)\exp\left(\mathbb{A}t\right)=\exp\left[\left(\mathbb{A}^{\dagger}+\mathbb{A}+\frac{1}{2}\left[\mathbb{A},\mathbb{A}^{\dagger}\right]+\cdots\right)t\right] \tag{1.36}$$

where the dots imply terms with more complicated commutators, such as $\left[\mathbb{A},\left[\mathbb{A},\mathbb{A}^{\dagger}\right]\right]$, $\left[\mathbb{A}^{\dagger},\left[\mathbb{A},\left[\mathbb{A},\mathbb{A}^{\dagger}\right]\right]\right]$ and so on.

It can be proven (see for example Ioannou [6]) that (1.35) generalizes to:

$$\sigma_{\min}\leq e^{\Re(\lambda_i)t}\leq\sigma_{\max}\quad\text{for every eigenvalue }\lambda_i\text{ of }\mathbb{A} \tag{1.37}$$

In this case the eigenvectors of $e^{\mathbb{A}^{\dagger}t}e^{\mathbb{A}t}$ do not coincide with those of $\mathbb{A}$ or $\mathbb{A}^{\dagger}$.

Often we are interested in the growth of perturbations in the limit of large time and at small times. We would like to know how we can attain

maximum growth in these two limits, and which initial state achieves it.

We can always (see Appendix A) write an arbitrary vector as:

$$\mathbf{y} = \sum_{i=1}^{N} \frac{\left(\mathbf{v}^{(i)}, \mathbf{y}\right)}{\left(\mathbf{v}^{(i)}, \mathbf{u}^{(i)}\right)} \mathbf{u}^{(i)} \tag{1.38}$$

If we furthermore we assume that eigenvectors have been sorted in descending order of the real part of their eigenvalues, then, in the limit $t \to \infty$ we have, from equation (1.38), that:

$$\mathbf{y} \to \frac{\left(\mathbf{v}^{(1)}, \mathbf{y}\right)}{\left(\mathbf{v}^{(1)}, \mathbf{u}^{(1)}\right)} e^{\lambda^R_{\max} t} \mathbf{u}^{(1)}$$

So the maximum growth rate is:

$$\sigma^2(t) = \frac{\left(\mathbf{y}(t)\,,\, \mathbf{y}(t)\right)}{\left(\mathbf{y}(0), \mathbf{y}(0)\right)} \to e^{2\lambda^R_{\max} t} \frac{\left(\mathbf{u}^{(1)}, \mathbf{u}^{(1)}\right)}{\left|\left(\mathbf{v}^{(1)}, \mathbf{u}^{(1)}\right)\right|^2} \frac{\left|\left(\mathbf{v}^{(1)}, \mathbf{y}(0)\right)\right|^2}{\left(\mathbf{y}(0), \mathbf{y}(0)\right)}$$

from which it is obvious that at this limit, the initial condition that will achieve $\sigma^{+\infty}_{\max}$ is the corresponding eigenvector of the adjoint operator $\mathbf{y}(0) = \mathbf{v}^{(1)}$.

Concerning the limit $t \to 0$ we can expand $e^{\mathbb{A}^\dagger t} e^{\mathbb{A} t}$ in powers of t as:

$$e^{\mathbb{A}^\dagger t} e^{\mathbb{A} t} = \mathbb{1} + \left(\mathbb{A} + \mathbb{A}^\dagger\right) t + \mathcal{O}\left(t^2\right) \tag{1.39}$$

Thus we can see that the maximum initial growth rate is achieved by the maximum eigenvalue λ of the hermitian operator $\left(\mathbb{A} + \mathbb{A}^\dagger\right)/2$ with corresponding $\sigma^0_{\max} = 1 + \lambda t$. The state that produces instantaneously this maximum growth rate is the corresponding eigenvector of $\left(\mathbb{A} + \mathbb{A}^\dagger\right)/2$.

1.5 Pseudospectra

The concept of pseudospectra is closely related with non-normality. We will be dealing in this Section with matrices but all of these concepts can be easily generalized to infinite dimensional differential operators. For a more detailed reference on the subject see Trefethen and Embree [12].

The spectrum of a matrix $\mathbb{A} \in \mathbb{C}^{N\times N}$ is defined as the set of complex numbers $\lambda \in \mathbb{C}$ such that for some vectors $\mathbf{u} \in \mathbb{C}^N$ we have $A\mathbf{u} = \lambda\mathbf{u}$. Equivalently we can say that spectrum is the set of complex numbers $\lambda \in \mathbb{C}$ such that the matrix $(\mathbb{A} - \lambda\mathbb{1})$ does not have an inverse, or that the resolvent matrix $(\lambda\mathbb{1} - \mathbb{A})^{-1}$ is infinite.

There are various definitions of pseudospectra. We will give two of them here.

Definition 1.5.1 (Pseudospectra #1). *For a matrix $\mathbb{A} \in \mathbb{C}^{N\times N}$ the ε-pseudospectra $\Lambda_\varepsilon(\mathbb{A})$, $\varepsilon > 0$, is the set $z \in \mathbb{C}$ such that*[3]*:*

$$\| (z - \mathbb{A})^{-1} \| > \varepsilon^{-1} \tag{1.40}$$

Where by $\|\cdot\|$ we mean the Euclidean 2-norm defined in (1.33). Also, we use the convention that $\| (z - \mathbb{A})^{-1} \| = \infty = \Lambda_0(\mathbb{A})$ for $z \in \Lambda(\mathbb{A})$. Another definition of the pseudospectra is:

Definition 1.5.2 (Pseudospectra #2). *For a matrix $\mathbb{A} \in \mathbb{C}^{N\times N}$ the ε-pseudospectra $\Lambda_\varepsilon(\mathbb{A})$, $\varepsilon > 0$, is the set $z \in \mathbb{C}$ such that:*

$$z \in \Lambda(\mathbb{A} + \mathbb{E}) \tag{1.41}$$

for some $\mathbb{E} \in \mathbb{C}^{N\times N}$ with $\|\mathbb{E}\| < \varepsilon$.

[3] we will from now on omit the $\mathbb{1}$ whenever there is no possibility of confusion

The first of the two definition defines the ε-pseudospectrum as the open subset of the complex plane bounded by the ε^{-1} level curve of the norm of the resolvent. The spectrum is of course contained in the ε-pseudospectrum for every $\varepsilon > 0$. The second definition defines the ε-pseudospectrum as the set of eigenvalues of the perturbed matrix $\mathbb{A} + \mathbb{E}$ for a perturbations with norm $\|\mathbb{E}\| < \varepsilon$. Again according to this definition the spectrum is contained in the ε-pseudospectrum for every $\varepsilon > 0$. For a theorem that proves the equivalence of the above definitions see Theorem 2.1 of [12].

Also from the definitions it follows that pseudospectra associated with different ε are nested sets, that is:

$$\Lambda(\mathbb{A}) \subset \Lambda_{\varepsilon_1}(\mathbb{A}) \subseteq \Lambda_{\varepsilon_2}(\mathbb{A}) \quad \text{for} \quad 0 < \varepsilon_1 \leq \varepsilon_2 \tag{1.42}$$

The second definition provides a more useful physical interpretations. For physical situations where all the dynamical variables are not known and we are forced to proceed to approximate description of our physical system, the concept of ε-pseudospectrum can show as the sensitivity of the eigenvalues. For normal matrices the ε-pseudospectrum will be the union of circles of radius ε in the complex plane, with centers the eigenvalues of the matrix (Theorem 2.2 of [12]). This means (in view of definition #2) that if we perturb the matrix by ε-normed matrix its eigenvalues will lie ε distance away in the complex plane. This in not at all true for non-normal matrices, where an ε-normed perturbation of the matrix can move the eigenvalues very much.

1.6 Construction of the adjoint perturbation system

The adjoint operator [4] L_{adj} will be defined using the inner product

$$(f,g) = \int dt \int dx \int dz \ \left[\frac{1}{2}\left(u_f^* u_g + w_f^* w_g\right) + \frac{1}{2} J \left(-\frac{\mathrm{d}\rho_0}{\mathrm{d}z} \right) \eta_f^* \eta_g \right] \tag{1.43}$$

where $f = [u_f, w_f, \varrho_f, p_f]^{\mathrm{T}}$, $g = [u_g, w_g, \varrho_g, p_g]^{\mathrm{T}}$. In the chosen variables this inner product corresponds to total perturbation energy integrated over time. The adjoint operator is defined by:

$$\Big((L_{\text{adj}}\psi), \phi \Big) = \Big(\psi, L\phi \Big) \tag{1.44}$$

To obtain the adjoint system we multiply equations (1.10) respectively by $[u_\alpha, w_\alpha, \eta_\alpha, p_\alpha]$ and integrate by parts over t, x and z. Assuming that the fields vanish at the boundary of the space-time domain we obtain immediately the adjoint operator:

$$L_{\text{adj}} = \begin{bmatrix} -\left(\partial_t + U_0 \partial_x\right) & 0 & 0 & -\partial_x \\ \mathrm{d}U_0/\mathrm{d}z & -\left(\partial_t + U_0 \partial_x\right) & J\left(\mathrm{d}\rho_0/\mathrm{d}z\right) & -\partial_z \\ 0 & 1 & -\left(\partial_t + U_0 \partial_x\right) & 0 \\ -\partial_x & -\partial_z & 0 & 0 \end{bmatrix} \tag{1.45}$$

or equivalently the adjoint system:

$$\left(\frac{\partial}{\partial t} + U_0 \frac{\partial}{\partial x} \right) u_\alpha = -\frac{\partial p_\alpha}{\partial x} \tag{1.46.a}$$

$$\left(\frac{\partial}{\partial t} + U_0 \frac{\partial}{\partial x} \right) w_\alpha = \frac{\mathrm{d}U_0}{\mathrm{d}z} u_\alpha + J \frac{\mathrm{d}\rho_0}{\mathrm{d}z} \eta_\alpha - \frac{\partial p_\alpha}{\partial z} \tag{1.46.b}$$

$$\left(\frac{\partial}{\partial t} + U_0 \frac{\partial}{\partial x} \right) \eta_\alpha = w_\alpha \tag{1.46.c}$$

$$\frac{\partial u_\alpha}{\partial x} + \frac{\partial w_\alpha}{\partial z} = 0 \tag{1.46.d}$$

By introducing a streamfunction for describing the adjoint perturbation velocity field, as equation (1.13), we can reduce our adjoint systems (1.46) to:

$$\frac{\partial \mathbf{x}_\alpha}{\partial t} = \mathbb{A}_{\text{adj}}\, \mathbf{x}_\alpha \tag{1.47}$$

where $\mathbf{x}_\alpha = [\psi_\alpha, \eta_\alpha]^{\mathrm{T}}$ is our state vector, or one can proceed furthermore and reduce the system into the adjoint Taylor-Goldstein second order differential equation for ψ_α:

$$\left(\frac{\partial}{\partial t} + U_0 \frac{\partial}{\partial x}\right)^2 \Delta\psi_\alpha + 2\frac{\mathrm{d}U_0}{\mathrm{d}z}\left(\frac{\partial}{\partial t} + U_0\frac{\partial}{\partial x}\right)\mathrm{D}\frac{\partial \psi_\alpha}{\partial x} - J\frac{\mathrm{d}\rho_0}{\mathrm{d}z}\frac{\partial^2 \psi_\alpha}{\partial x^2} = 0 \tag{1.48}$$

where D denotes the partial derivative $\partial/\partial z$.

If we proceed with decomposition in Fourier space for x-domain, as with system (1.15), then the system (1.47) can be written as:

$$\frac{d}{dt}\mathbf{x}_{\alpha\, k} = \mathbb{A}^{(k)}_{\text{adj}}\, \mathbf{x}_{\alpha\, k} \tag{1.49}$$

where $\mathbb{A}^{(k)}_{\text{adj}}$ is the (differential) adjoint of the dynamical operator $\mathbb{A}^{(k)}$,

$$\mathbb{A}^{(k)}_{\text{adj}} = \begin{bmatrix} \Delta^{-1}\left(-ikU_0\Delta - 2ik\dfrac{\mathrm{d}U_0}{\mathrm{d}z}\mathrm{D}\right) & -ikJ\Delta^{-1}\dfrac{\mathrm{d}\rho_0}{\mathrm{d}z} \\ -ik & -ikU_0 \end{bmatrix} \tag{1.50}$$

Modal dependance for x and t domains, of the form $e^{ik(x-ct)}$, is assumed. Thus, all quantities can be written as:

$$\varphi(x,z,t) = \int_{-\infty}^{+\infty} dc \int_{-\infty}^{+\infty} dk\; \hat{\varphi}_{ck}(z) e^{ik(x-ct)} \tag{1.51}$$

and of course it is again assumed that the real part must be taken for variables representing physical quantities.

In this modal representation the Taylor-Goldstein equation, (1.17), defines an eigenvalue problem. We know that if c is an eigenvalue of (1.17) then c^* must be an eigenvalue of the adjoint equation,(1.48) (see definition of adjoint operator, (1.44)). With this we can proceed and ask what is the relation of ψ and ψ_α corresponding to the complex conjugate pair of c and c^*. We impose modal dependance of (1.51) of the form:

$$\varphi_\alpha(x,z,t) = \int_{-\infty}^{+\infty} dc \int_{-\infty}^{+\infty} dk\ \hat{\varphi}_{\alpha\, ck}(z) e^{ik(x-c^*t)} \tag{1.52}$$

at (1.48) we can see then that if $\hat{\psi}_{ck}$ is a solution of (1.17) then $\hat{\psi}^*_{ck}/\left(U_0 - c^*\right)$ satisfies (1.48). From (1.46.c) we have that the adjoint mode corresponding to:

$$\mathbf{x}_{ck} = \begin{bmatrix} \hat{\psi}_{ck} \\ \\ \hat{\eta}_{ck} \end{bmatrix}$$

is given by:

$$\mathbf{x}_{\alpha\, ck} = \begin{bmatrix} \dfrac{\hat{\psi}^*_{ck}}{U_0 - c^*} \\ \\ -\dfrac{\hat{\eta}^*_{ck}}{U_0 - c^*} \end{bmatrix} \tag{1.53}$$

1.7 Orthogonality relation

In the energy metric our dynamical operator $\mathbb{A}$ is non-normal. It is known [3] that when an operator $\mathbb{A}$ in non-normal its eigenfunctions are not orthogonal. However, there are orthogonal to the eigenfunctions of its adjoint, that correspond to eigenvalues different from the complex conjugate of the former.

To obtain the bi-orthogonality relations we note that if $\phi = [u, w, \eta, p]^{\mathrm{T}}$ satisfies the equations (1.10) and $\phi_\alpha = [u_\alpha, w_\alpha, \eta_\alpha, p_\alpha]^{\mathrm{T}}$ the adjoint equa-

tions (1.46), then the following continuity equation derives:

$$\partial_t \varepsilon + \partial_x J_x + \partial_z J_z = 0 \ , \tag{1.54}$$

with

$$\varepsilon = \frac{1}{2}\left(u_\alpha^* u + w_\alpha^* w\right) + \frac{1}{2} J \left(-\frac{\mathrm{d}\rho_0}{\mathrm{d}z}\right) \eta_\alpha^* \eta \tag{1.55}$$

and

$$J_x = U_0 \varepsilon + p_\alpha^* u + u_\alpha^* p \tag{1.56}$$

$$J_z = p_\alpha^* w + w_\alpha^* p \tag{1.57}$$

$$\tag{1.58}$$

For this two dimensional problem we define:

$$\langle \phi_a, \phi \rangle = \int_{-\infty}^{\infty} \varepsilon \, dz \quad , \quad [\phi_a, \phi] = \int_{-\infty}^{\infty} J_x \, dz \quad . \tag{1.59}$$

The continuity equation (1.54) then gives, upon using vanishing boundary conditions at $|z| \to \infty$:

$$\partial_t \langle \phi_a, \phi \rangle + \partial_x [\phi_a, \phi] = 0 \ . \tag{1.60}$$

Let us now consider modal harmonic perturbations of the form $\phi = \hat{\phi}_{ck} \, e^{ik(x-ct)}$ and $\phi_a = \hat{\phi}_{a\,c'k'} \, e^{ik'(x-c't)}$ with k and k' real, then (1.60), using (1.27), gives:

$$(k'c'^* - kc) \left\langle \hat{\phi}_{a\,c'k'}, \hat{\phi}_{ck} \right\rangle = (k' - k) \left[\hat{\phi}_{a\,c'k'}, \hat{\phi}_{ck} \right] \ . \tag{1.61}$$

Consequently considering modes with the same k that correspond to phase

velocities $c \neq c'^*$ satisfy the biorthogonality relation:

$$\left\langle \hat{\phi}_{a\,c'k}, \hat{\phi}_{ck} \right\rangle = 0 \quad \text{for} \quad c \neq c'^* \tag{1.62}$$

This inner product produces a square norm that corresponds to the energy density of a mode.

Chapter 2

Applications

2.1 Holmboe's classical problem

We will continue by analyzing a simple problem first analyzed by Holmboe and try to acquire a better understanding of the concepts of Sections 1.4, 1.6 and 1.7. We will study the piecewise velocity and density profiles:

$$U_0(z) = \begin{cases} 1/2 & : \quad z > 1/2 \\ z & : \quad -1/2 \leq z \leq 1/2 \\ -1/2 & : \quad z < -1/1 \end{cases} \tag{2.1.a}$$

$$\rho_0(z) = \begin{cases} -d/2 & : \quad z > 0 \\ d/2 & : \quad z < 0 \end{cases} \tag{2.1.b}$$

We plot them in Figure 2.1.

We separate the z-domain into four distinct areas: area 1: $z > 1/2$, area 2: $0 < z < 1/2$, area 3: $-1/2 < z < 0$ and area 4: $z < -1/2$. In all of these areas we have that $U_0'' = \rho_0' = 0$ and that is ψ, according to (1.17), must be a harmonic function. Since periodicity in x-domain is assumed, we can expand all fields in fourier space in x-domain as (1.26). Thus we

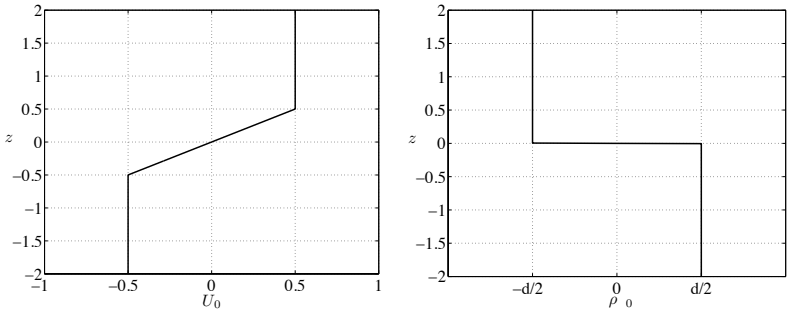

2.1(a): main velocity profile $U_0(z)$ (eq. (2.1.a))

2.1(b): main density profile $\rho_0(z)$ (eq. (2.1.b))

Figure 2.1: Main piecewise profiles of (2.1).

have[1]:

$$\hat{\psi}_1(z,t) = A_1(t)e^{-k(z-1/2)} \tag{2.2.a}$$

$$\hat{\psi}_2(z,t) = A_2(t)e^{-kz} + B_2(t)e^{kz} \tag{2.2.b}$$

$$\hat{\psi}_3(z,t) = A_3(t)e^{-kz} + B_3(t)e^{kz} \tag{2.2.c}$$

$$\hat{\psi}_4(z,t) = B_4(t)e^{k(z+1/2)} \tag{2.2.d}$$

where zero boundary conditions at $z = \pm\infty$ have been imposed. The value of the η field must be continuous in the whole domain. In view of (1.10.c), and since U_0 is continuous, we deduce that ψ must be continuous. Thus we have the following boundary conditions for the streamfunction:

[1] the k subscript is being neglected where not necessary to distinguish between different streamwise wavenumbers

$$\hat{\psi}_1(z,t) - \hat{\psi}_2(z,t)\Big|_{z=1/2} = 0 \tag{2.3.a}$$

$$\hat{\psi}_2(z,t) - \hat{\psi}_3(z,t)\Big|_{z=0} = 0 \tag{2.3.b}$$

$$\hat{\psi}_3(z,t) - \hat{\psi}_4(z,t)\Big|_{z=-1/2} = 0 \tag{2.3.c}$$

If we define $C_2(t) = (A_2(t) + B_2(t))\, e^{k/2}$ we can use the above boundary conditions to reduce the number of unknowns of equations (2.2) from six to three. Moreover, we demand that the total pressure to be continuous over the three separation surfaces. This consists of:

$$P_0(z+\eta) + p(x, z+\eta, t)$$

which when linearized for small values of η gives:

$$P_0(z) + \eta \frac{\mathrm{d}P_0}{\mathrm{d}z} + p(x,z,t)$$

The main pressure field P_0 is continuous and furthermore is connected to the main density field through the hydrostatic relation[2], $\mathrm{d}P_0/\mathrm{d}z = -(J/d)$. This results that the quantity:

$$p(x,z,t) - (J/d)\,\eta(x,z,t) \tag{2.4}$$

must be continuous. In the modal representation (1.26) the value of $\hat{p}$ can be derived from the u-momentum equation. Thus we have that at

[2] in the Boussinesq approximation

the three surface the quantity:

$$\frac{1}{-ik}\left[\left(\partial_t + U_0\partial_x\right)\mathrm{D}\hat{\psi} + U_0'\left(-ik\hat{\psi}\right)\right] - \left(J/d\right)\hat{\eta} \tag{2.5}$$

should be continuous. Thus we get three equations for $A_1(t)$, $C_2(t)$ and $B_4(t)$ which together with $\eta_0(t) \equiv \hat{\eta}(z=0,t)$ give the following dynamical system:

$$\frac{d}{dt}\,\mathbb{K}\,\mathbf{u} = \mathbb{L}\,\mathbf{u} \tag{2.6}$$

where $\mathbf{u} = [A_1(t)\ \ C_2(t)\ \ B_4(t)\ \ \eta_0(t)]^{\mathrm{T}}$ and:

$$\mathbb{K} = \begin{bmatrix} -e^k & 1 & 0 & 0 \\ 2 & -2\left(1+e^{-k}\right) & 2 & 0 \\ 0 & 1 & -e^k & 0 \\ 0 & 0 & 0 & 1 \end{bmatrix} \tag{2.7.a}$$

$$\mathbb{L} = \begin{bmatrix} \frac{i}{2}\left(1+e^k(k-1)\right) & -\frac{i}{2}k & 0 & 0 \\ 0 & 0 & 0 & -iJ\left(e^{k/2}-e^{-k/2}\right) \\ 0 & \frac{i}{2}k & -\frac{i}{2}\left(1+e^k(k-1)\right) & 0 \\ 0 & -ike^{-k/2} & 0 & 0 \end{bmatrix} \tag{2.7.b}$$

and with the rest of the coefficients given by:

$$A_2(t) = \frac{1}{e^{k/2}-e^{-k/2}}\left[C_2(t) - A_1(t)\right] \tag{2.8.a}$$

$$A_3(t) = \frac{1}{e^{k/2}-e^{-k/2}}\left[B_4(t) - e^k C_2(t)\right] \tag{2.8.b}$$

$$B_2(t) = \frac{1}{e^{k/2}-e^{-k/2}}\left[A_1(t) - e^{-k} C_2(t)\right] \tag{2.8.c}$$

$$B_3(t) = \frac{1}{e^{k/2}-e^{-k/2}}\left[B_4(t) - C_2(t)\right] \tag{2.8.d}$$

The energy of the perturbations according to (1.28) will be given by:

$$E = T + V = \int_{-\infty}^{+\infty} dz \left[\frac{1}{4} \left(|\mathrm{D}\hat{\psi}|^2 + k^2 |\hat{\psi}|^2 \right) + \frac{1}{4} \frac{J}{d} \left(-\frac{\mathrm{d}\rho_0}{\mathrm{d}z} \right) |\hat{\eta}|^2 \right] \tag{2.9}$$

Since the discontinuity in the main density field the term gradient of the main density field becomes $\mathrm{d}\rho_0/\mathrm{d}z = -d\,\delta(z)$ and thus the integral of the potential energy give only contribution from $z = 0$:

$$P = \frac{1}{4} J \, |\eta_0|^2 \tag{2.10}$$

The integral of the kinetic energy is broken into four parts. In each area we have:

$$\int_a^b dz \, \frac{1}{4} \left(|\mathrm{D}\hat{\psi}|^2 + k^2 |\hat{\psi}|^2 \right) = \frac{1}{4} \, \hat{\psi}^* \, \mathrm{D}\hat{\psi} \Big|_a^b \tag{2.11}$$

since $\Delta\psi_i = 0$, $i = 1, 2, 3, 4$. Thus kinetic energy integral becomes:

$$\begin{aligned} T = & \frac{1}{4} \times \left(-\hat{\psi_1}^* \, \mathrm{D}\hat{\psi_1} \Big|_{z=h/2} + \hat{\psi_2}^* \, \mathrm{D}\hat{\psi_2} \Big|_{z=h/2} - \hat{\psi_2}^* \, \mathrm{D}\hat{\psi_2} \Big|_{z=0} \right) \\ & + \frac{1}{4} \times \left(\hat{\psi_3}^* \, \mathrm{D}\hat{\psi_3} \Big|_{z=0} - \hat{\psi_3}^* \, \mathrm{D}\hat{\psi_3} \Big|_{z=-h/2} + \hat{\psi_4}^* \, \mathrm{D}\hat{\psi_4} \Big|_{z=-h/2} \right) \end{aligned} \tag{2.12}$$

This induces a metric of the form:

$$\mathbb{M} = \frac{1}{4} \begin{bmatrix} \mathbb{M}_\mathrm{T} & 0 \\ 0 & J \end{bmatrix} \tag{2.13}$$

where $\mathbb{M}_\mathrm{T}$ is:

$$\mathbb{M}_\mathrm{T} = \frac{2k}{(e^k - 1)} \begin{bmatrix} e^k & -1 & 0 \\ -1 & 1 + e^{-k} & -1 \\ 0 & -1 & e^k \end{bmatrix} \tag{2.14}$$

In terms of Section 1.4 we have that:

$$\mathbb{A} = \mathbb{K}^{-1}\mathbb{L} \tag{2.15}$$

$$\mathbb{A}_{\mathrm{M}} = \mathbb{M}^{1/2}\mathbb{A}\mathbb{M}^{-1/2} \tag{2.16}$$

At first the modal stability of system (2.6) is analyzed. In Figure 2.2 we present the maximum modal growthrates of operator $\mathbb{A}_{\mathrm{M}}$, kc_i, $c_i = \Im(c)$, versus the streamwise wavenumber, k and the bulk Richarson number J. The unstable modes come in pairs with the same growth rate kc_i and opposite phase velocities $c_r \equiv \Re(c)$. A slice of this contour plot for $J = 0.25$ is depicted in Figure 2.3. Also the spectrum of $\mathbb{A}_{\mathrm{M}}$ together with the ε-pseudospectrum is seen in Figure 2.4. We can see that, as mentioned in Section 1.5, due to the non-normality of $\mathbb{A}_{\mathrm{M}}$ the boundaries of the ε-pseudospectra do not lie in circles around the eigenvalues of radius equal to ε, but to rather larger distances.

We next plot in Figure 2.5 the maximum energy that can be attained in every value of t together with the energy of the evolution of the most unstable mode[3]. The former is given by $\|e^{\mathbb{A}_{\mathrm{M}}t}\|^2$ (where the Euclidean norm is understood here). We make plots for $J = 0.25$ two values of streamwise wavenumber, $k = 0.25$ and $k = 1.75$. The latter refers to the area where maximum Holmboe instability occurs (see Figure 2.2) and the former to an area where there the flow is modally stable. Some interesting things arrise here. Notice at first, that the energy of the evolution of each of the most unstable modes. The $k = 0.25$ does not increase at all, being a stable mode with $kc_i = 0$, while the $k = 1.75$ case increases exponentially with time. However take a look at the optimal energy that

[3]There are in general two mostly unstable modes with opposite phase velocities. Here we draw the energy evolution of one of them.

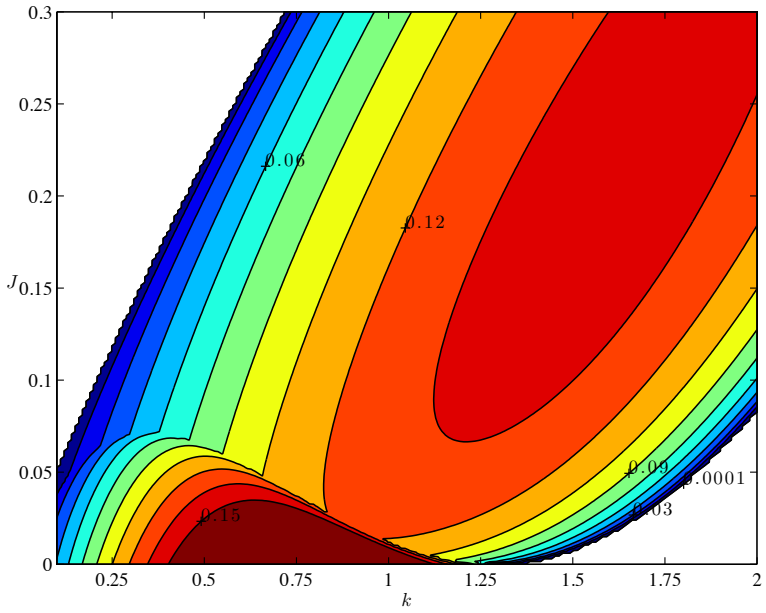

Figure 2.2: Nondimensional modal growth rate kc_i of $\mathbb{A}_{\mathrm{M}}$ of (2.16) vs streamwise wavenumber and bulk Richarson number for linear, normal mode instabilities of the main profile of (2.1).

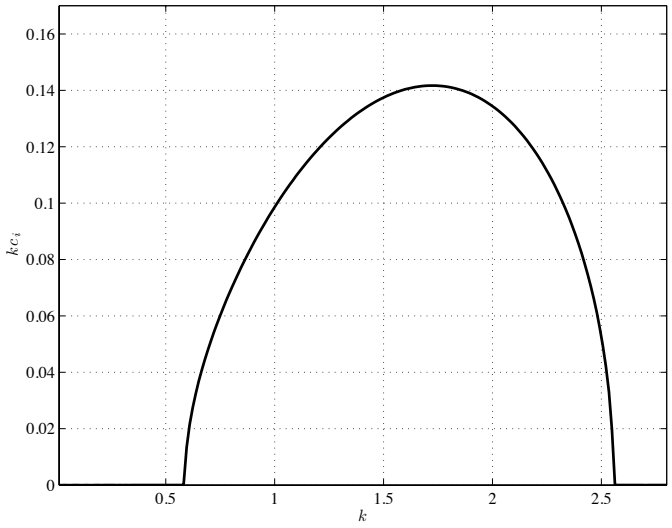

Figure 2.3: Maximum modal instability for various values of streamwise wavenumber k of $\mathbb{A}_{\mathrm{M}}$ of (2.16) for $J = 0.25$. We can see that instability lies between two values of k_{min} and k_{max} of k.

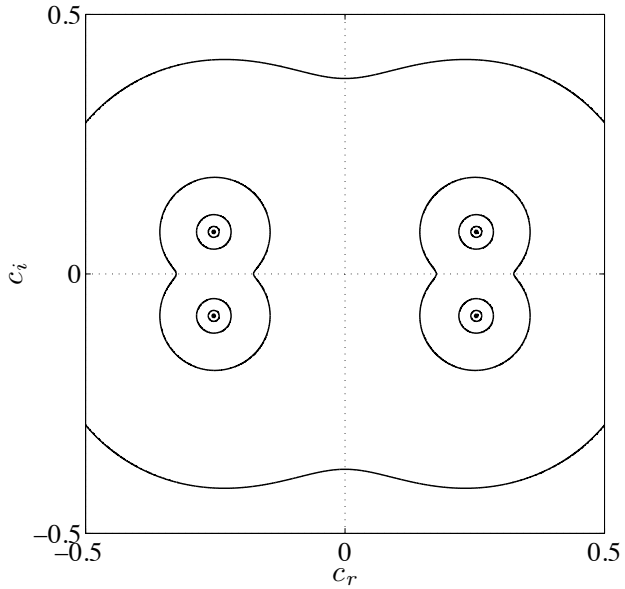

Figure 2.4: The spectrum of $\mathbb{A}_{\mathrm{M}}$ for $k = 1.75$ and $J = 0.25$ together ε-pseudospectra. Eigenvalues are shown with dots while boundaries of the 2-norm of ε-pseudospectra are shown with solid lines for $\varepsilon = 10^{-0.5}, 10^{-1.0}, 10^{-1.5}, 10^{-2.0}$ (from outer to inner). We can see clearly that as ε grows, the ε-pseudospectrum boundaries do not form circles of radius ε but cover much bigger areas.

can be achieved at each instant. Fot the $k = 1.75$ case the optimal in very close to the energy achieved by the unstable mode. In the case of $k = 0.25$ though, optimal energy evolution is not constant. We see an increase of the same order as of that of the unstable case. Up to 10 advective time units we cannot almost distinguish between the optimal of the unstable or the stable mode. We see that we can get up to 10 times energy increment with no modal instability at all. This is achieved thought the non-normal interaction between the non-orthogonal modes of the dynamical operator.

In Figure 2.6 we plot for $J = 0.25$ the structures of the unstable modes and their corresponding adjoints for the two values of streamwise wavenumber mentioned above. We also plot the optimal structures for $T_{\text{opt}} = 8$.

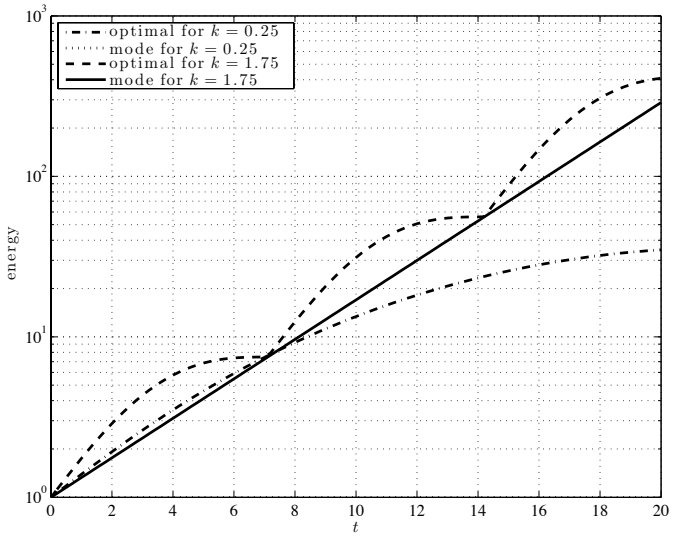

Figure 2.5: Maximum energy that can be attained in every value of t, given by $\|e^{\mathbb{A}_{\mathrm{M}}t}\|^2$, together with the energy of the evolution of the most unstable mode (either one of the two) for $J = 0.25$ and streamwise wavenumber $k = 0.25$ (modally stable) and $k = 1.75$ (modally unstable). Notice that the optimal energy that can be achieved at each instant for $k = 1.75$ is very close to the energy achieved by the unstable mode. However, for $k = 0.25$ increases of the same order as of that of the unstable case. We see that we can get up to 10 times energy increment with no modal instability at all.

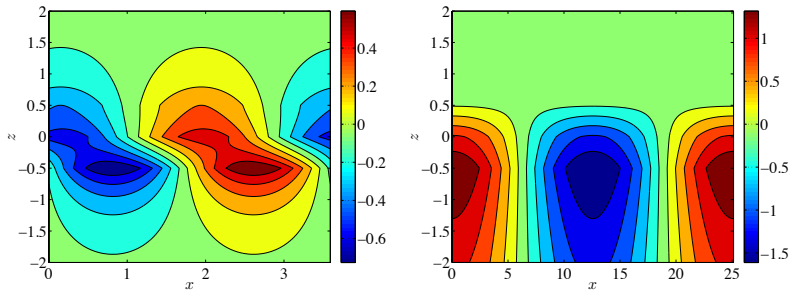

2.6(a): $\hat{\psi}$ of unstable eigenmode, $k = 1.75$

2.6(b): $\hat{\psi}$ of unstable eigenmode, $k = 0.25$

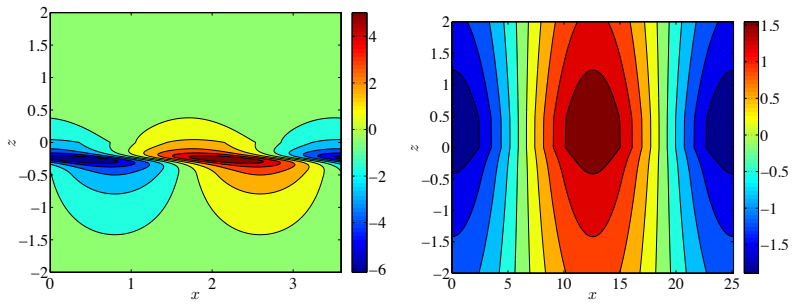

2.6(c): $\hat{\psi}_\alpha$ of adjoint of unstable eigenmode, $k = 1.75$

2.6(d): $\hat{\psi}_\alpha$ of adjoint of unstable eigenmode, $k = 0.25$

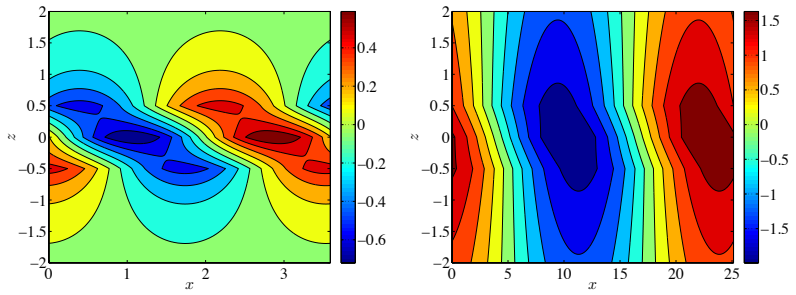

2.6(e): $\hat{\psi}$ of optimal excitation for $T_{\text{opt}} = 8$, $k = 1.75$

2.6(f): $\hat{\psi}$ of optimal excitation for $T_{\text{opt}} = 8$, $k = 0.25$

Figure 2.6: Contour plots for $J = 0.25$ of one member of the pair of the mostly unstable eigenmodes of the system and for (a) $k = 1.75$ and (b) $k = 0.25$, and its corresponding adjoint mode (c) $k = 1.75$ and (d) $k = 0.25$. Also the optimal structures for $T_{\text{opt}} = 8$ for (e) $k = 1.75$ and (f) $k = 0.25$. Notice that while the mostly unstable and its adjoint for $k = 0.25$ have their contours neither slope forward nor backward ($kc_i = 0$), the optimal for $T_{\text{opt}} = 8$ for $k = 0.25$ has its contours slope backwards and thus results to increase of energy (see Figure 1.7(b)).

2.2 Holmboe smoothed profiles

In the previous section we have seen that non-normal interaction between the modes of the system can lead to a substantial transient energy growth even in the absence of modal instability (Figure 2.5). However, in the previous sections we have ignored the continuous spectrum of the operator. The last of course plays no significant role if one is concerned with the modal stability of the system, since the continuous spectum is always real and within the region of the main velocity profile (for a proof refer to [2]). However, there is no reason why interaction of the non-orthogonal modes of the system should constrict only among the discrete ones. We will now numerically approach the same problem incuding now both the discrete and the continuous part of the spectrum and see how big gain of energy we can gain from the this interaction.

We will study the problem of main velocity and density profiles with hyperbolic tangent dependance on z. More specifically (also ploted in Figure 2.7):

$$U_0(z) = \frac{1}{2}\tanh(2z - \beta) \tag{2.17.a}$$

$$\rho_0(z) = -\frac{1}{2}\tanh(2Rz) \tag{2.17.b}$$

The parameter R now measures the ratio of the shear layers in velocity and dentisy, while β is a measure of the assymetry of the two profiles and will be considered zero, (symmetric profiles, $\beta = 0$) until explicitly said. We can see that the piecewise profiles (2.1) studied earlier are not but a mere idealization of these ones for limit of very high values of R.

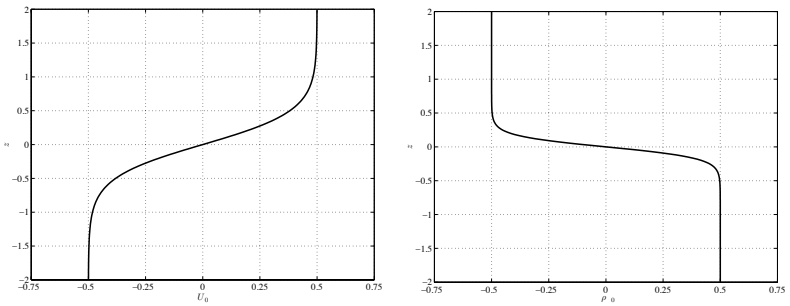

2.7(a): main velocity profile $U_0(z)$ 2.7(b): main density profile $\rho_0(z)$

Figure 2.7: Main velocity profile (a) and main density profile (b) with shear ratio $R = 3$.

The (dimensional) Brunt-Väisälä frequency, N^* is:

$$\begin{aligned} N^{*2}(z^*) &= -g\frac{\mathrm{d}\rho_0^*/\mathrm{d}z^*}{\rho_m^*} \\ &= \frac{g\tilde{\rho}}{\rho_m^* h_0}\left(-\frac{\mathrm{d}\rho_0}{\mathrm{d}z}\right) \\ &\equiv N_0^{*2}\, R\,\mathrm{sech}^{\,2}\left(R\frac{2z^*}{h_0}\right) \end{aligned} \tag{2.18}$$

while the Richarson number is defined as the Brunt-Väisälä frequency squared over the local shear squared,

$$\begin{aligned} \mathrm{Ri}(z) &= -g\frac{\mathrm{d}\rho_0^*/\mathrm{d}z^*}{\rho_m^*\left(\mathrm{d}U_0^*/\mathrm{d}z^*\right)^2} \\ &= \frac{gR\tilde{\rho}h_0}{\rho_m^*\tilde{u}^2}\frac{\mathrm{sech}^{\,2}\left(2Rz\right)}{\mathrm{sech}^{\,4}\left(2z-\beta\right)} \\ &\equiv \mathrm{Ri}_0\frac{\mathrm{sech}^{\,2}\left(2Rz\right)}{\mathrm{sech}^{\,4}\left(2z-\beta\right)} \end{aligned} \tag{2.19}$$

where ρ_m^* is the mean background density and if we use the previous definition of J, (1.6), we have that $J = \mathrm{Ri}_0/R$. Also the non-dimensional Brunt-Väisälä frequency $N^2(z)$ is defined to be:

$$N^2(z) \equiv \frac{N^{*2}(z^*)}{N_0^{*2}} = R\,\mathrm{sech}^{\,2}(2Rz) \tag{2.20}$$

With these conventions and also with the use of η as a variable (see (1.9)), our dynamical system (1.5) takes the form (1.10):

$$\left(\frac{\partial}{\partial t}+U_0\frac{\partial}{\partial x}\right)u=-\frac{\mathrm{d}U_0}{\mathrm{d}z}w-\frac{\partial p}{\partial x} \tag{2.21.a}$$

$$\left(\frac{\partial}{\partial t}+U_0\frac{\partial}{\partial x}\right)w=-\frac{\partial p}{\partial z}-JN^2(z)\eta \tag{2.21.b}$$

$$\left(\frac{\partial}{\partial t}+U_0\frac{\partial}{\partial x}\right)\eta=w \tag{2.21.c}$$

$$\frac{\partial u}{\partial x}+\frac{\partial w}{\partial z}=0 \tag{2.21.d}$$

where:

$$\frac{\mathrm{d}U_0}{\mathrm{d}z}=\operatorname{sech}^2(2z-\beta) \tag{2.22.a}$$

$$\frac{\mathrm{d}\rho_0}{\mathrm{d}z}=-N^2(z)=-R\operatorname{sech}^2(2z-\beta) \tag{2.22.b}$$

At first the modal stability of the corresponding system (1.15) produced by the above equations with the specific main profiles is analyzed. In Figure 2.8 and Figure 2.9 we present the maximum modal growthrates of operator $\mathbb{A}_{\mathrm{M}}$, kc_i, $c_i=\Im(c)$, versus the streamwise wavenumber, k and the center Richarson number. In the first of the two figures the ratio of the shear zones is kept fixed at $R=3$ and J is varied. We can see that there is not much difference from the piecewise case, Figure 2.2 (where R was infinite). Again we can easily distinguish the two branches of Kelvin-Helmholtz instability and Holmboe. However, this becomes much more clear in Figure 2.9 where J is kept fixed at $J=0.15$ and the ratio of the shear zones, R is varied (agreement with results of Smyth and Winters [8] is established). We can see clearly that there are two branches sepearated by $\mathrm{Ri}_0=0.25$. The lower branch corresponds to Kelvin-Helmholtz instability where the unstable mode is only one and its phase velocity is zero,

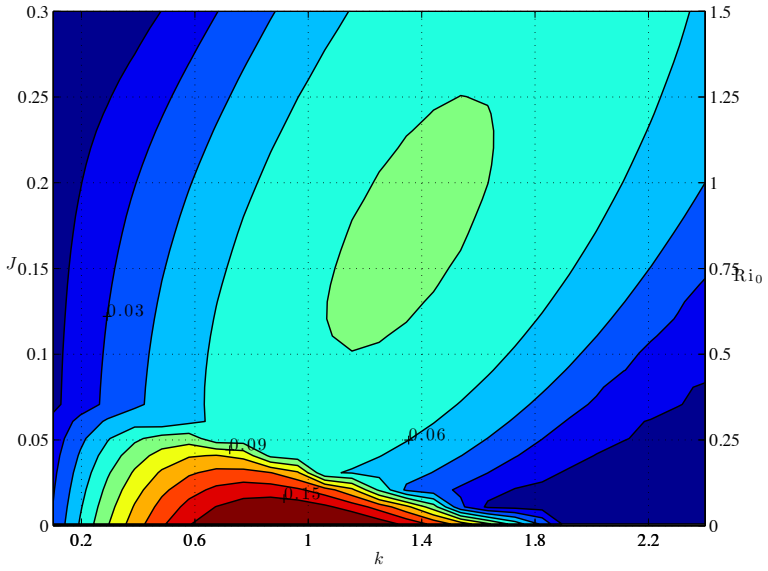

Figure 2.8: Nondimensional modal growth rate kc_i of $\mathbb{A}_{\mathrm{M}}$ for main profiles of (2.17) versus streamwise wavenumber and Richarson number for linear, normal mode instabilities of an inviscid stratified shear layer for fixed $R = \mathrm{Ri}_0/J = 5$. The domain depth $L_z = 4$.

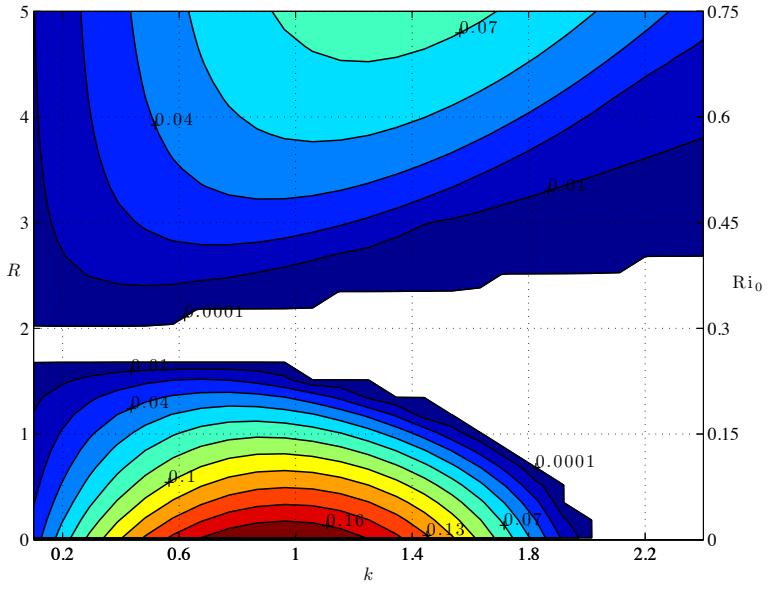

Figure 2.9: Nondimensional modal growth rate kc_i of $\mathbb{A}_{\mathrm{M}}$ for main profiles of (2.17) versus streamwise wavenumber and shear ratio Richarson number for linear, normal mode instabilities of an inviscid stratified shear layer for fixed $J = \mathrm{Ri}_0/R = 0.15$. The domain depth $L_z = 4$.

$c_r = \Re(c) = 0$. The upper branch corresponds to the so called Holmboe waves. The unstable modes come in pairs with non-zero, opposite phase velocities. Thus, if $R < 2$ the Holmboe waves do not appear.

We will consider the Holmboe case and therefore from now on work at $R = 3$ and $J = \mathrm{Ri}_0/R = 0.15$ and also with streamwise wavenumber $k = 0.8$ which corresponds very near to the maximum modal growth attained in this Richarson number (as can be seen more clearly in Figure 2.12). The spectrum for these specific set of parameters is plotted in Figure 2.10.

In Figure 2.11(a) we plot the spectrum together with the ε-pseudospectra of the operator $\mathbb{A}_\mathrm{M}$ for an area around one of the unstable modes (top right one seen on Figure 2.10), while in Figure 2.11(b) we plot the same but for a normal operator, here denoted by $\mathbb{A}_\mathrm{M}^{(\mathrm{N})}$ that has exactly the same spectrum with $\mathbb{A}_\mathrm{M}$. The latter is easily constructed by considering a diagonal operator formed from the eigenvalues of $\mathbb{A}_\mathrm{M}$. We see that the boundaries of the ε-pseudospectra for $\mathbb{A}_\mathrm{M}^{(\mathrm{N})}$ are circles around the eigenvalues of radius ε, while this does not hold of $\mathbb{A}_\mathrm{M}$. We also notice that for $\mathbb{A}_\mathrm{M}$ the same contours of ε extend in much more greater areas around the eigenvalues than for $\mathbb{A}_\mathrm{M}^{(\mathrm{N})}$ (the outer contour lines in both figures correspond to the same value of ε).

In Figure 2.13 we plot for $k = 0.8$, $R = 3$ and $J = \mathrm{Ri}_0/R = 0.15$ the contour plots of the structures of the $\hat{\psi}$ and $\hat{\eta}$ for the most unstable eigenmode of the system (2.13(a) and 2.13(b)), its corresponding adjoint mode (2.13(c) and 2.13(d)) and the structure that achieves maximum initial growth, $\sigma^0_{\max}$ (2.13(e) and 2.13(f)). Next, in Figure 2.14 we plot for the same values of parameters k, R and J, the evolution of energy of the unstable eigenmode of the system, its corresponding adjoint, the state of maximum instantaneous growth and the state that gives the op-

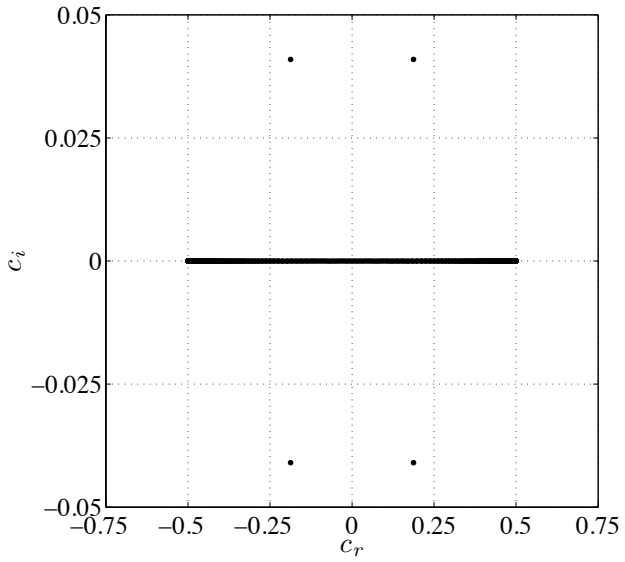

Figure 2.10: Spectrum of $\mathbb{A}_{\mathrm{M}}$ for $k = 0.8$, $R = 3$ and $J = 0.15$. We can see clearly the four discrete modes (two pairs of stable and unstable modes with opposite phase velocities) and also the continuous part of the spectrum with phase velocities $\min(U_0) \leq c_r \leq \max(U_0)$.

timal growth at $T = 30$ together with the maximum energy that can be attained at any time t, that is $\|\exp(\mathbb{A}_{\mathrm{M}} t)\|^2$. We notice that after 50 time units the evolution is almost parallel. The unstable mode has dominated. However, starting with the adjoint mode has gained energy almost two orders of magnitude more. Also one can see that indeed the eigenmode of $\left(\mathbb{A}_{\mathrm{M}} + \mathbb{A}_{\mathrm{M}}^{\dagger}\right)/2$ with larger eigenvalue corresponds to the maximum instantaneous growth.

We next plot in Figure 2.15 the maximum energy that can be attained in every value of t for various values of streamwise wavenumber k for $R = 3$ and $J = 0.15$. Some interesting things arrise here. Up to 30 time units one can achieve the same order of magnitude energy growth with wavenumbers ranging from $k = 0.2$ to $k = 2$. This fact seems counterintuitive if we try to interpret it only with means of Figure 2.12

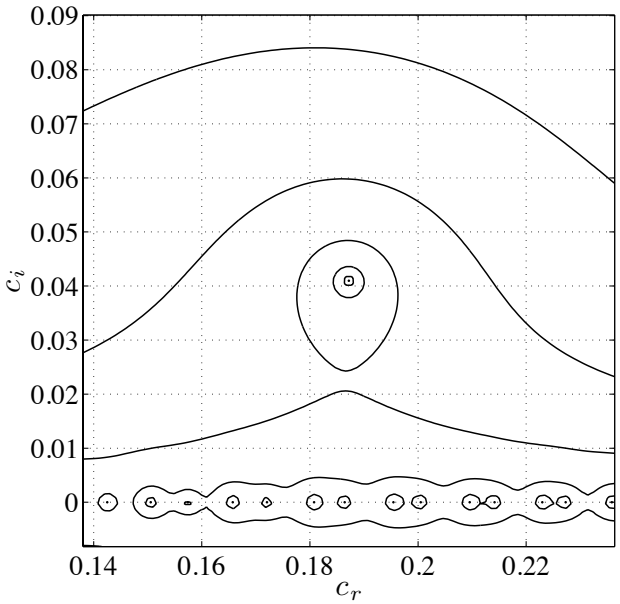

2.11(a): ε-pseudospectra of $\mathbb{A}_{\mathrm{M}}$

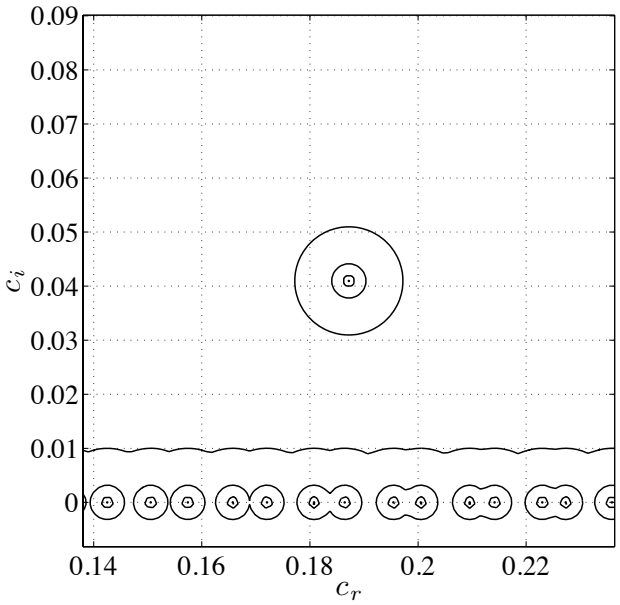

2.11(b): ε-pseudospectra $\mathbb{A}_{\mathrm{M}}^{(\mathrm{N})}$

Figure 2.11: Pseudospectra of $\mathbb{A}_{\mathrm{M}}$ and of the normal operator $\mathbb{A}_{\mathrm{M}}^{(\mathrm{N})}$ for $k = 0.8$, $R = 3$ and $J = 0.15$ for the area near one of the discrete modes. Plot shows the eigenvalues (solid dots) and the boundaries of the 2-norm ε-pseudospectra for $\varepsilon = 10^{-2.0}, 10^{-2.5}, 10^{-3.0}, 10^{-3.5}, 10^{-4.0}$ (from outer to inner). We see that the ε-pseudospectrum for $\mathbb{A}_{\mathrm{M}}^{(\mathrm{N})}$ are circles around the eigenvalues of radius ε, while this does not hold of $\mathbb{A}_{\mathrm{M}}$. Notice that for $\mathbb{A}_{\mathrm{M}}$ the same contours of ε extend in much more greater areas around the eigenvalues than for $\mathbb{A}_{\mathrm{M}}^{(\mathrm{N})}$, where the contours for $\varepsilon = 10^{-3.5}, 10^{-4.0}$ are so close to the eigenvalues that cannot be distinguished.

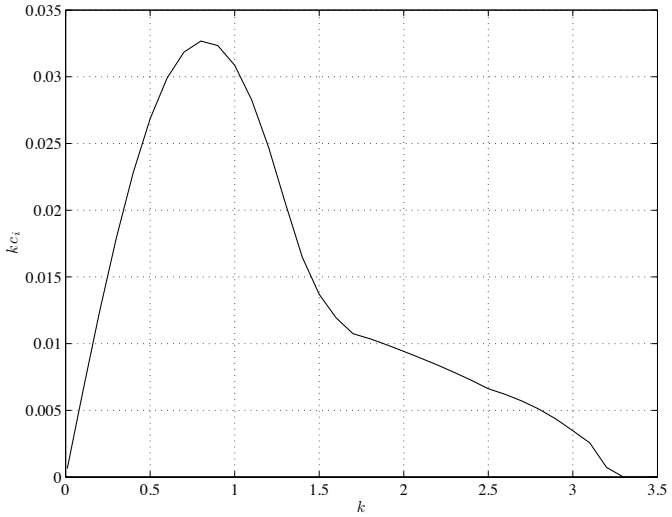

Figure 2.12: Maximum modal growth rate kc_i of $\mathbb{A}_{\mathrm{M}}$ for main profiles of (2.17) versus streamwise wavenumber k, for $J = 0.15$ and $R = 3$. The domain depth $L_z = 4$. We can see that $k = 0.8$ is very near to the maximum achieved modal growth rate.

and modal stability terms. One would expect for example almost three times more exponential growth for $k = 0.8$ than for $k = 2$. However, though the non-normal interaction between the non-orthogonal modes of the dynamical operator of discrete and continuous part of the spectrum we have the same growth for this two values of streamwise wavenumber.

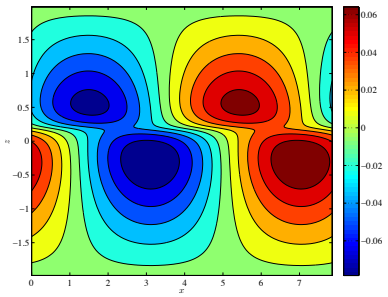

2.13(a): $\hat{\psi}$ of unstable eigenmode

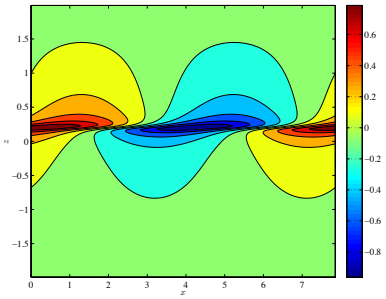

2.13(b): $\hat{\eta}$ of unstable eigenmode

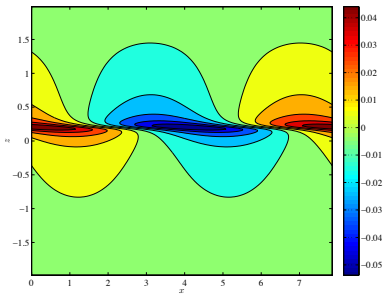

2.13(c): $\hat{\psi}_\alpha$ of adjoint of unstable eigenmode

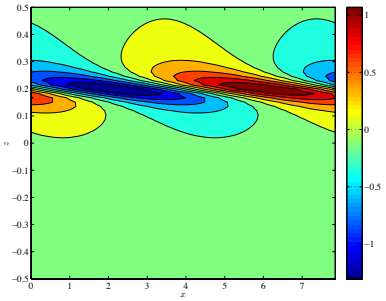

2.13(d): $\hat{\eta}_\alpha$ of adjoint of unstable eigenmode

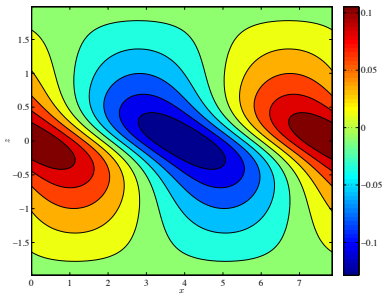

2.13(e): $\hat{\psi}$ of of eigenmode of $\left(\mathbb{A}_\mathrm{M} + \mathbb{A}_\mathrm{M}^\dagger\right)/2$

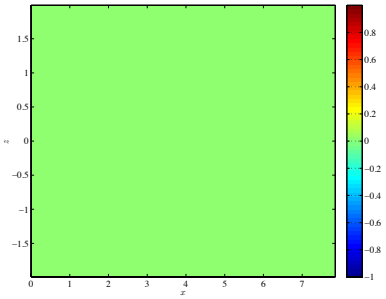

2.13(f): $\hat{\eta}$ of eigenmode of $\left(\mathbb{A}_\mathrm{M} + \mathbb{A}_\mathrm{M}^\dagger\right)/2$

Figure 2.13: Contour plots of one of the most unstable eigenmode of the system (a) and (b) and its corresponding adjoint mode (c) and (d). Streamwise wavenumber is $k = 0.8$, $R = 3$ and $J = \mathrm{Ri}_0/R = 0.15$. The domain depth $L_z = 4$. We. Notice the z scale difference in the η_α adjoint field.

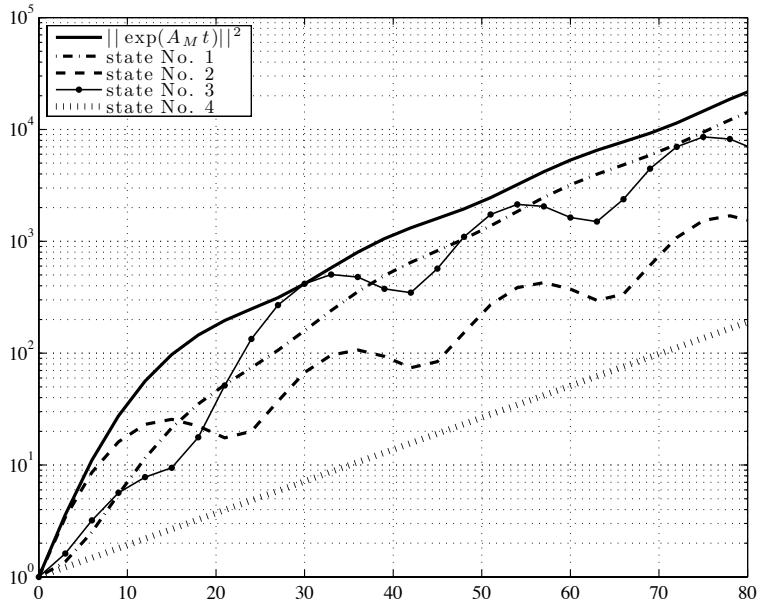

Figure 2.14: The evolution of energy of the unstable eigenmode of the system (state No. 1 - dotted line), its corresponding adjoint (state No. 2 - dash-dot line), the state of maximum instantaneous growth (state No. 3 - dashed line) and the state that gives the optimal growth at $T = 30$ (state No. 4 - solid doted line). Also in the figure is the plot of the maximum energy that can be attained at any time t (solid line). Streamwise wavenumber is $k = 0.8$ and $J = \mathrm{Ri}_0/R = 0.15$. Notice that after 50 time units the evolution is almost parallel. The unstable mode has dominated. However, starting with the adjoint mode has gained energy almost two orders of magnitude more.

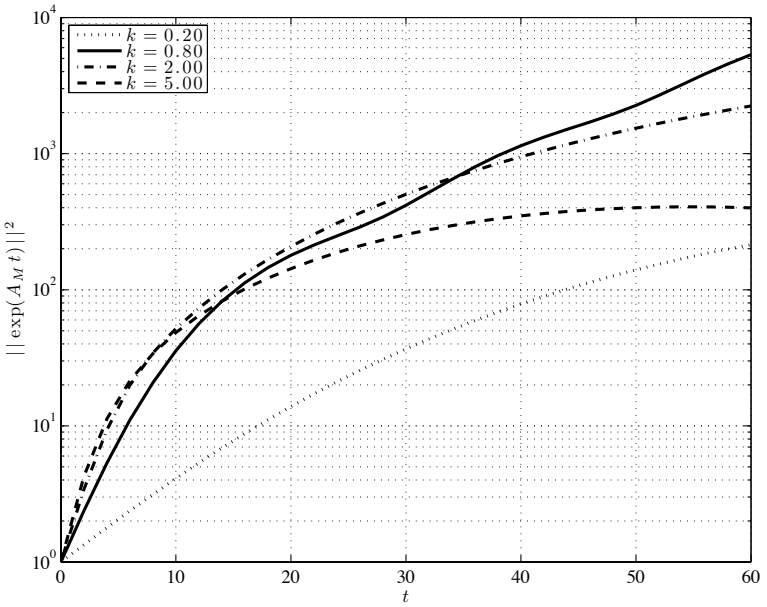

Figure 2.15: The optimal growth as a function of time for different values of streamwise wavenumber, k. Notice that in the transient period (less than 35 advective time units) the wavenumber that corresponds to the maximum modal growth does not give the overall maximum optimal energy growth.

Chapter 3

Conclusions

We have reviewed (Section 1.1) the main hydrodynamic instability mechanism for unidirectional flows that vary only in the cross-stream direction, i.e. the basic hydrodynamic shear instabilities. These are the Kelvin-Helmholtz instability (stratified and unstratified), the Rayleigh instability, the Taylor instability and finally the Holmboe instability. The most counterintuitive of these is the Holmboe, because it demonstrates against intuition that the stratification may act as a *destabilizing* factor for streamwise wavenumbers that are otherwise stable, in contrast with the stratified Kelvin-Helmholtz case.

The hydrodynamic perturbation equations are non-normal because energy can flow from the background mean to the perturbations. As a result the stability analysis must go beyond the analysis of the spectrum of the operator. We have reviewed the methods required to address the stability of non-normal dynamical systems. We have shown by example that non-normality is able to produce energy growths for streamwise wavenumbers that are neutral and excite the unstable modes at orders of magnitude higher amplitude by initializing the dynamical system by the

adjoint mode rather than unstable mode itself (see Figures 2.5 and 2.15). We found that a study of the instability of non-normal dynamical systems should be extended to include a study of the norm of the propagator which may reveal stability characteristics that are very different from the ones expected from modal stability analysis, which always underestimates the sensitivity of fluid flows.

We have also shown that the eigenspectrum of non-normal operators when it exists is ill-conditioned and very sensitive. We introduced the methods of pseudo-spectral analysis to investigate the sensitivity of the spectra. We proposed that the best basis for analysis of non-normal operators is the polar decomposition of the propagator, that leads to the singular value decomposition of the operator that identifies two unitary bases which can provide not only a good basis for expansion the perturbation field, but also a physically compelling basis because these unitary structures are the structures of the flow that are ordered according to their growth potential. We have applied these ideas to the Holmboe problem.

Appendices

A Adjoint operator properties

We will assume for this section that inner product is the usual Eucledian $(\mathbf{u}, \mathbf{v}) \equiv \mathbf{u}^\dagger \mathbf{v}$.

Let a linear operator $\mathbb{A}$ acting on an N-dimensional vector space, V, with eigenvalues λ_i and eigenvectors $\mathbf{u}^{(i)}$, that is:

$$\mathbb{A}\,\mathbf{u}^{(i)} = \lambda_i\,\mathbf{u}^{(i)} \tag{A.1}$$

Its adjoint operator, $\mathbb{A}^\dagger$, is defined as equation (1.30).

Theorem A.1. *The eigenspectrum of $\mathbb{A}$ and $\mathbb{A}^\dagger$ are complex conjugates, that is:*

$$\lambda_i \in \Lambda(\mathbb{A}) \Longleftrightarrow \lambda_i^* \in \Lambda(\mathbb{A}^\dagger) \tag{A.2}$$

Proof. If we denote by μ_i and $\mathbf{v}^{(i)}$ the eigenvalues and eigenvectrors of $\mathbb{A}^\dagger$ then we have that:

$$\begin{aligned} \left(\mathbf{v}^{(j)}, \mathbb{A}\,\mathbf{u}^{(i)}\right)^* &= \left(\mathbf{u}^{(i)}, \mathbb{A}^\dagger\,\mathbf{v}^{(j)}\right) = \mu_j \left(\mathbf{u}^{(i)}, \mathbf{v}^{(j)}\right) \\ \left(\mathbf{v}^{(j)}, \mathbb{A}\,\mathbf{u}^{(i)}\right)^* &= \lambda_i^* \left(\mathbf{v}^{(j)}, \mathbf{u}^{(i)}\right)^* = \lambda_i^* \left(\mathbf{u}^{(i)}, \mathbf{v}^{(j)}\right) \end{aligned} \tag{A.3}$$

In another basis, $\left\{e^{(i)}\right\}_{i=1}^N$, these two operators have matrix elements:

$$A_{ij} = \left(e^{(i)}, \mathbb{A}\, e^{(j)}\right)$$
$$\left(A^\dagger\right)_{ij} = \left(e^{(i)}, \mathbb{A}^\dagger\, e^{(j)}\right)$$

thus

$$\left(A^\dagger\right)_{ij} = (A)^*_{ji}$$

Moreover:

$$\begin{aligned}\det\left(\mathbb{A}^\dagger\right) &= \sum_{i_1,i_2,\ldots,i_N} \epsilon_{i_1 i_2 \cdots i_N} (A^\dagger)_{i_1 1} (A^\dagger)_{i_2 2} \cdots (A^\dagger)_{i_N N} \\ &= \sum_{i_1,i_2,\ldots,i_N} \epsilon_{i_1 i_2 \cdots i_N} A^*_{1\, i_1} A^*_{2\, i_2} \cdots A^*_{N\, i_N} \\ &= (\det \mathbb{A})^*\end{aligned}$$

This, accompanied from the fact that $[\det(\lambda \mathbb{1})]^* = \det(\lambda^* \mathbb{1})$, leads to:

$$0 = \det\left(\mathbb{A}^\dagger - \mu \mathbb{1}\right) = [\det(\mathbb{A} - \mu^* \mathbb{1})]^* = 0$$

which proofs (A.2). □

Going back to equation (A.3) we have:

$$(\lambda_i - \lambda_j)\left(\mathbf{v}^{(j)}, \mathbf{u}^{(i)}\right) = 0$$

or for $\lambda_i \neq \lambda_j$

$$\left(\mathbf{v}^{(j)}, \mathbf{u}^{(i)}\right) = 0 \tag{A.6}$$

If now we want to expand an arbitrary vector $\mathbf{y}$ into eigenvectos of $\mathbb{A}$ we

write:

$$\mathbf{y} = \sum_{i=1}^{N} \alpha_i \, \mathbf{u}^{(i)}$$

and to find the coefficients α_i we take the inner product with $\mathbf{v}^{(j)}$. This gives us:

$$\mathbf{y} = \sum_{i=1}^{N} \frac{\left(\mathbf{v}^{(i)}, \mathbf{y}\right)}{\left(\mathbf{v}^{(i)}, \mathbf{u}^{(i)}\right)} \mathbf{u}^{(i)} \tag{A.8}$$

which leads to the completeness relations:

$$\mathbb{1} = \sum_{i=1}^{N} \frac{\mathbf{u}^{(i)} \, \mathbf{v}^{(i)\dagger}}{\mathbf{v}^{(i)\dagger} \, \mathbf{u}^{(i)}} = \sum_{i=1}^{N} \frac{\mathbf{v}^{(i)} \, \mathbf{u}^{(i)\dagger}}{\mathbf{u}^{(i)\dagger} \, \mathbf{v}^{(i)}} \tag{A.9}$$

Theorem A.2. *A normal operator has a complete set of orthonormal eigenvectors.*

This does not hold if the operator is non-normal.

Proof. When the operator $\mathbb{A}$ is normal then:

$$\mathbb{A}^\dagger \mathbb{A} \, \mathbf{u}^{(i)} = \lambda_i \mathbb{A}^\dagger \, \mathbf{u}^{(i)} = \mathbb{A} \left(\mathbb{A}^\dagger \, \mathbf{u}^{(i)} \right) \qquad \square$$

That is if $\mathbf{u}^{(i)}$ is an eigenvector of $\mathbb{A}$ with eigenvalue λ_i, then so is $\mathbb{A}^\dagger \, \mathbf{u}^{(i)}$. In the case of no degeneracy, and due to (A.2) we conclude that in this case $\mathbf{u}^{(i)}$ is also an eigenvector of $\mathbb{A}^\dagger$ with eigenvalue λ_i^*. Otherwise, if $\mathbb{A}$ is degenerate and an n-dimensional eigenspace corresponds to eigenvalue λ_k then $\mathbb{A}^\dagger$ will also be degenerate and also an n-dimensional eigenspace will correspond to eigenvalue λ_k. Consenquently the previous relations

for biorthogonality and completeness become:

$$\begin{aligned} \left(\mathbf{u}^{(i)}, \mathbf{u}^{(j)}\right) &= \delta_{ij} \left(\mathbf{u}^{(i)}, \mathbf{u}^{(i)}\right) \\ \sum_{i=1}^{N} \frac{\mathbf{u}^{(i)}\, \mathbf{u}^{(i)\dagger}}{\mathbf{u}^{(i)\dagger}\, \mathbf{u}^{(i)}} &= \mathbb{1} \end{aligned}$$

B Singular value decomposition

Theorem B.1. *Every operator $\mathbb{A}$ admits singular value decomposition into:*

$$\mathbb{A} = \mathbb{U}\mathbb{\Sigma}\mathbb{V}^\dagger$$

where $\mathbb{U}$ and $\mathbb{V}$ are unitary operators and $\mathbb{\Sigma}$ is diagonal with positive entries.

The values σ_i in the diagonal of $\mathbb{\Sigma}$ are called singular values and normally are ordered in descending order, $\sigma_1 \geq \sigma_2 \geq \cdots \geq \sigma_N$.

Proof. The hermitian operators $\mathbb{A}\mathbb{A}^\dagger$ and $\mathbb{A}^\dagger\mathbb{A}$ are positive since:

$$\left(\mathbf{x}, \mathbb{A}\mathbb{A}^\dagger\mathbf{x}\right) = \left(\mathbb{A}^\dagger\mathbf{x}, \mathbb{A}^\dagger\mathbf{x}\right) \geq 0$$
$$\left(\mathbf{x}, \mathbb{A}^\dagger\mathbb{A}\,\mathbf{x}\right) = \left(\mathbb{A}\,\mathbf{x}, \mathbb{A}\,\mathbf{x}\right) \geq 0$$

Then the hermitian operator $\mathbb{H} = \left(\mathbb{A}^\dagger\mathbb{A}\right)^{1/2}$ can be defined as:

$$\mathbb{H} = \mathbb{V}\sqrt{\mathbb{S}}\mathbb{V}^\dagger$$

where $\mathbb{S}$ is the diagonal matrix with the eigenvalues of $\mathbb{A}^\dagger\mathbb{A}$ in its diagonal and $\mathbb{V}$ is the unitary matrix whose columns are the eigenvectors of $\mathbb{A}^\dagger\mathbb{A}$. Then $\mathbb{\Phi} \equiv \mathbb{A}\mathbb{H}^{-1}$ is unitary since:

$$\mathbb{\Phi}^\dagger\mathbb{\Phi} = \left(\mathbb{A}\mathbb{H}^{-1}\right)^\dagger \mathbb{A}\mathbb{H}^{-1} = \mathbb{H}^{-1}\mathbb{A}^\dagger\mathbb{A}\mathbb{H}^{-1} = \mathbb{H}^{-1}\mathbb{H}^2\mathbb{H}^{-1} = \mathbb{1}$$
$$\mathbb{\Phi}\mathbb{\Phi}^\dagger = \mathbb{A}\mathbb{H}^{-1}\left(\mathbb{A}\mathbb{H}^{-1}\right)^\dagger = \mathbb{A}\mathbb{H}^{-1}\mathbb{H}^{-1}\mathbb{A}^\dagger = \mathbb{A}\left(\mathbb{A}^\dagger\mathbb{A}\right)^{-1}\mathbb{A}^\dagger = \mathbb{1}$$

Consequently, every operator $\mathbb{A}$ can be written as:

$$\mathbb{A} = \mathbb{\Phi}\mathbb{H} \tag{B.1}$$

where $\mathbb{\Phi}$ is unitary and $\mathbb{H}$ is hermitian. This is called polar decomposition of an operator, it is in the manner of defining a complex number by a magnification by an amplitude (a hermitian matrix here) and then a rotation by $e^{i\phi}$, where ϕ is the phase (a unitary matrix here).

We let $\mathbb{\Sigma}$ be the diagonal operator with elements the square roots of the elements of $\mathbb{S}$. Then, rewriting (B.1),

$$\mathbb{A} = \mathbb{\Phi V \Sigma V}^\dagger$$

Note that the unitarity of $\mathbb{\Phi}$ implies that if v_1 and v_2 are two orthogonal vectors then also are $\mathbb{\Phi}v_1$ and $\mathbb{\Phi}v_2$, thus $\mathbb{\Phi V}$ is also unitary (unitary matrices form a group) .

But also from (B.1) we induce that:

$$\begin{aligned}
\mathbb{AA}^\dagger &= \mathbb{\Phi H} \left(\mathbb{\Phi H}\right)^\dagger = \mathbb{\Phi H H}^\dagger \mathbb{\Phi}^\dagger \\
&= \mathbb{\Phi} \left(\mathbb{V}\sqrt{\mathbb{S}}\mathbb{V}^\dagger\right) \left(\mathbb{V}^\dagger\sqrt{\mathbb{S}}\mathbb{V}\right) \mathbb{\Phi}^\dagger \\
&= \left(\mathbb{\Phi V}\right) \mathbb{S} \left(\mathbb{\Phi V}\right)^\dagger
\end{aligned}$$

Thus the unitary matrix $\mathbb{U} \equiv \mathbb{\Phi V}$ is the matrix whose columns are the eigenvectors of $\mathbb{AA}^\dagger$. □

We now not only have the proof that any operator $\mathbb{A}$ can be decomposed into $\mathbb{A} = \mathbb{U\Sigma V}^\dagger$, but we also have the way of doing it. Moreover, equation (B.1) has also shown us that any operator can be decomposed into a unitary and a hermitian one. The latter is called polar decomposition of an operator.

C Miles & Howard criterion

Theorem C.1 (Miles & Howard). *A parallel, stratified, inviscid flow with the local Richarson number everywhere greater than* $1/4$ *is stable under infinitesimal perturbations.*

We will give here follow the proof given by Howard [5] together with the assumption of the Boussinesq approximation, so we will be consistent with the rest of our text. However, this approximation plays no significant role in the proof and the theorem holds for any initial configuration of the density ρ_0 with slight modifications.

Proof. From Taylor-Goldstein equation, (1.17), if we expand the stream-function as (1.51) and also define $F(z)$ as:

$$\hat{\psi}(z) = (U_0 - c)\, F(z) \tag{C.1}$$

we end up with:

$$\begin{aligned} \left[(U_0 - c)^2 F'\right]' + \left[-J\frac{\mathrm{d}\rho_0}{\mathrm{d}z} - k^2 (U_0 - c)^2\right] F = 0 \\ \left[(U_0 - c)^2 F'\right]' + \left[\left(U_0'\right)^2 \mathrm{Ri} - k^2 (U_0 - c)^2\right] F = 0 \end{aligned} \tag{C.2}$$

since in this notation, the local Richarson number is given by:

$$\mathrm{Ri}(z) = \frac{-J\mathrm{d}\rho_0/\mathrm{d}z}{(\mathrm{d}U_0/\mathrm{d}z)^2} \tag{C.3}$$

Let us now assume that the flow is unstable to infinitesimal perturbations, that is $c_i > 0$ and also that $\mathrm{Ri}(z) > 1/4$ for the whole z-domain. Let us further denote $W(z) = U_0(z) - c$ and since $c_i > 0$ it means that W does not have a zero in the flow domain and thus we can select one branch of

$W^{1/2}$ for the whole domain. If we furthermore denote $G(z) = W^{1/2}F(z)$ then equation (C.2) becomes:

$$\left(WG'\right)' - \left[\frac{1}{2}U_0'' + k^2 W + \frac{\left(U_0'\right)^2}{W}\left(\frac{1}{4} - \mathrm{Ri}\right)\right] G = 0 \tag{C.4}$$

We multiply with G^* and integrate in the whole z-domain. We have that $\hat{\psi}$ should vanish at the boundaries, which implies that G should vanish also. After the integration we end up with:

$$\int_{z_1}^{z_2} dz\, W\left(\left|G'\right|^2 + k^2\left|G\right|^2\right) + \int_{z_1}^{z_2} dz\, \frac{1}{2}U_0''\left|G\right|^2 + \int_{z_1}^{z_2} dz\, \left(U_0'\right)^2\left(\frac{1}{4} - \mathrm{Ri}\right) W^* \left|\frac{G}{W}\right|^2 = 0 \tag{C.5}$$

If we take the imaginary part of the above equation, and keep in mind that $c_i > 0$ then we end up with:

$$\int_{z_1}^{z_2} dz\, \left(\left|G'\right|^2 + k^2\left|G\right|^2\right) + \int_{z_1}^{z_2} dz\, \left(U_0'\right)^2\left(\mathrm{Ri} - \frac{1}{4}\right)\left|\frac{G}{W}\right|^2 = 0 \tag{C.6}$$

which cannot be true according to our assumptions. Thus we have that a sufficient condition for instability is that $\mathrm{Ri}(z) < 1/4$ for some z in the domain of the flow. □

Bibliography

[1] G. K. Batchelor. *An Introduction to Fluid Dynamics*. Cambridge University Press, Cambridge, third edition, 2000.

[2] P. G. Drazin and W. H. Reid. *Hydrodynamic Stability*. Cambridge University Press, Cambridge, 1981.

[3] B. F. Farrell and P. J. Ioannou. Generalized stability. Part I: Autonomous operators. *J. Atmos. Sci.*, 53:2025–2040, 1996.

[4] D. C. Hill. Adjoint systems and their role in the receptivity problem for boundary layers. *J. Fluid Mech.*, 292:183–204, 1995.

[5] L. N. Howard. Note on a paper of John W. Miles. *J. Fluid Mech.*, 10: 509–512, 1961.

[6] P. J. Ioannou. Non-normality increases variance. *J. Atmos. Sci.*, 52: 1155–1158, 1995.

[7] J. W. Miles. On the stability of heterogeneous shear flows. *J. Fluid Mech.*, 10:496–508, 1961.

[8] W. D. Smyth and K. B. Winters. Turbulence and mixing in Holmboe waves. *J. Phys. Oceanogr.*, 33(4):694–711, 2003.

[9] H. B. Squire. On the stability for three-dimensional disturbances of viscous fluid flow between parallel walls. *Proc. R. Soc. London, Ser. A*, 142(847):621–628, 1933.

[10] G. I. Taylor. Effect of variation in density on the stability of superposed streams of fluid. *Proc. R. Soc. London, Ser. A*, 132(820): 499–523, 1931.

[11] E. D. Tedford. *Laboratory, field and numerical investigations of Holmboe's instability*. PhD thesis, The University of British Columbia (Vancouver), 2009.

[12] L. N. Trefethen and M. Embree. *Spectra and pseudospectra: The behavior of nonnormal matrices and operators*. Princeton University Press, 2005.

[13] C.-S. Yih. Stability of two-dimensional parallel flows for three-dimensional disturbances. *Q. Appl. Math.*, 12(434), 1955.